Geochemistry Geophysics Geosystems G3
AN ELECTRONIC JOURNAL OF THE EARTH SCIENCES
Published by AGU and the Geochemical Society

Article
Volume 7, Number 2
2 February 2006
Q02002, doi:10.1029/2005GC001079
ISSN: 1525-2027

Constraints on Indian plate motion since 20 Ma from dense Russian magnetic data: Implications for Indian plate dynamics

S. Merkouriev
SPbFIZMIRAN, Muchnov per, 2, Box 188, St. Petersburg, 191023, Russia (sam@ns1480.spb.edu)

C. DeMets
Department of Geology and Geophysics, University of Wisconsin-Madison, Madison, Wisconsin, 53706, USA (chuck@geology.wisc.edu)

[1] We use more than 230,000 km of Russian marine magnetic and bathymetric data from the Carlsberg and northern Central Indian ridges, comprising one of the most geographically extensive, dense shipboard surveys anywhere in the ocean basins, to describe in detail seafloor spreading since 20 Ma along the trailing edge of the Indian plate. India-Somalia plate rotations for ~1 Myr intervals over the past 20 Myr are derived from inversions of more than 6600 crossings of 20 magnetic reversals and ~1400 crossings of fracture zones that offset these two ridges. Statistical analysis of the numerous data indicates that outward displacement of reversal boundaries due to finite seafloor emplacement widths and correlated noise for anomaly crossings from individual spreading segments constitute two distinct sources of systematic bias in the locations of magnetic anomaly crossings, contrary to the often-made assumption that random, Gaussian-distributed noise dominates the error budget. Seafloor spreading rates slowed gradually by 30% from 20 Ma to 10 ± 1 Ma about a relatively stationary pole of rotation. From 11 Ma to 9 Ma the rotation axis migrated several angular degrees toward the plate boundary, modestly increasing the spreading gradient along the plate boundary. India-Somalia kinematic data for times since ~9 Ma are consistent with remarkably steady motion, with no evidence for a change in either the rotation pole or rate of angular opening within the few percent precision of our data. The timing and nature of changes in India-Somalia motion since 20 Ma closely resemble those for the Capricorn-Somalia plate pair, indicating that India and Capricorn plate motions are strongly coupled. We speculate that the slowdown in seafloor spreading at the trailing edges of the Indo-Capricorn composite plate from 20 Ma to 10 ± 1 Ma resulted from the increasing amount of work that was needed to build topography in the Himalayan collisional zone. The transition to stable India-Somalia and Capricorn-Somalia seafloor spreading at ~10–9 Ma corresponds well with the onset at 8 Ma of folding and faulting across an equatorial plate boundary separating the Indian and Capricorn plates, suggesting that the latter may have played a fundamental role in restoring equilibrium between the torques that were driving and resisting the northward motions of the Indian and Capricorn plates.

Components: XXX words, 19 figures, 3 tables.

Keywords: India-Somalia motion; Indian plate dynamics; Tibetan plateau.

Index Terms: 3040 Marine Geology and Geophysics: Plate tectonics (8150, 8155, 8157, 8158); 8158 Tectonophysics: Plate motions: present and recent (3040).

Received 18 July 2005; **Revised** 4 October 2005; **Accepted** 23 November 2005; **Published** 2 February 2006.

Merkouriev, S., and C. DeMets (2006), Constraints on Indian plate motion since 20 Ma from dense Russian magnetic data: Implications for Indian plate dynamics, *Geochem. Geophys. Geosyst.*, *7*, Q02002, doi:10.1029/2005GC001079.

1. Introduction

[2] The collision of continental India and Eurasia at ~60–50 Ma was arguably the most important tectonic event of the Cenozoic Era, both for its tectonic effects and profound influence on the atmosphere, geosphere, and biosphere [*Molnar et al.*, 1993; *Molnar*, 2005]. The collision not only decreased the northward absolute motion of the Indian plate from a rapid 180–195 km Myr^{-1} before the collision to a more moderate 40–50 km Myr^{-1} afterward [*Klootwijk et al.*, 1991], but appears responsible for coeval slowdowns in seafloor spreading rates, changes in spreading directions, and spreading center reorganizations along the southern boundaries of the Indian plate [*Patriat and Achache*, 1984; *Patriat and Segoufin*, 1988]. Along the northern collisional boundary of the Indian plate, the uplift of the Himalayas and Tibetan plateau forced significant changes in the climate of the eastern hemisphere [e.g., *An et al.*, 2001; *Molnar*, 2005], and may have caused global cooling through enhanced weathering reactions that resulted in a long-term drawdown of atmospheric carbon dioxide [*Raymo and Ruddiman*, 1992; *Edmond and Huh*, 2003]. Increased outward forces acting on the lithosphere surrounding the growing Tibetan plateau may also have played a role in initiating folding and faulting at ~8 Ma of seafloor in the equatorial Central Indian basin [*Harrison et al.*, 1992; *Molnar et al.*, 1993].

[3] A key role of plate kinematic studies of the India-Eurasia collision has been to use the record of seafloor spreading along Indian plate boundaries to better establish the timing of major tectonic events affecting the Indian plate and if possible, gain insights into the evolution through time of the forces that drive and resist Indian plate motion. Prior to 1990, most studies of Indian plate motion focused on the nature of kinematic changes from 70–40 Ma, coinciding with the onset of continent-continent collision at the northern edge of the Indian plate [e.g., *Patriat and Achache*, 1984; *Molnar et al.*, 1988; *Patriat and Segoufin*, 1988]. More recent kinematic studies have focused increasingly on Indian plate motion since 20 Ma [*Wiens et al.*, 1985; *Gordon et al.*, 1990, 1998; *Royer and Chang*, 1991; *DeMets et al.*, 1994; *Royer et al.*, 1997], during which folding and faulting of an equatorial band of seafloor south of India began (~8 Ma) [*Moore et al.*, 1974; *Weissel et al.*, 1980; *Cochran*, 1990] and the Tibetan plateau likely rose to its present elevation [*Harrison et al.*, 1992; *Molnar et al.*, 1993].

[4] Using numerous marine magnetic data from the Central Indian ridge south of the India-Somalia-Capricorn triple junction, *DeMets et al.* [2005] (hereafter abbreviated DGR05) identify a significant change in Capricorn-Somalia motion at ~8 Ma, the same time within uncertainties as the onset of folding and faulting between the Indian and Capricorn plates. Their analysis of data from the northern Central Indian and Carlsberg ridges however reveals no evidence for significant changes in India-Somalia motion over the past 20 Ma, spanning the period when seafloor folding and faulting began (~8 Ma) in the equatorial Indian Ocean and when the Tibetan plateau likely increased to its maximum height. This raises the question of whether their result is merely an artifact of the sparse marine magnetic data that were available to DGR05 to constrain motion across the Carlsberg ridge.

[5] In this paper, we use a dense magnetic and bathymetric Russian survey of the Carlsberg and northern Central Indian ridges (Figures 1 and 2a) to study India-Somalia seafloor spreading since 20 Ma. With few or no parallels elsewhere along the mid-ocean ridge system, the extensive Russian survey covers more than 90% of the India-Somalia plate boundary, often to seafloor ages of 20 Ma (Figure 2a). The closely spaced survey tracks greatly facilitate the identification of individual magnetic anomalies and clearly define the segmentation of the paleo-ridge axis, both of which were important limiting factors in the DGR05 analysis.

[6] The principal goal of this paper is to test rigorously for the existence and timing of any post-20 Ma changes in India-Somalia motion. Such changes might be expected in light of the well-dated initiation of seafloor folding and faulting south of India at ~8 Ma and the likely rise of the Tibetan plateau to its present elevation during this period. To accomplish our goal, realistic estimates of uncertainties in our India-Somalia plate rotations and hence underlying data are essential. An important element of our analysis is thus to use the unusually numerous kinematic data to quantify random and systematic errors present in the plate kinematic data (section 4). In a series of carefully designed tests, we determine if errors in the locations of anomaly and fracture zone crossings are random and Gaussian-distributed (section 4.1), as has been assumed by ourselves and many previous authors when estimating uncertainties in plate

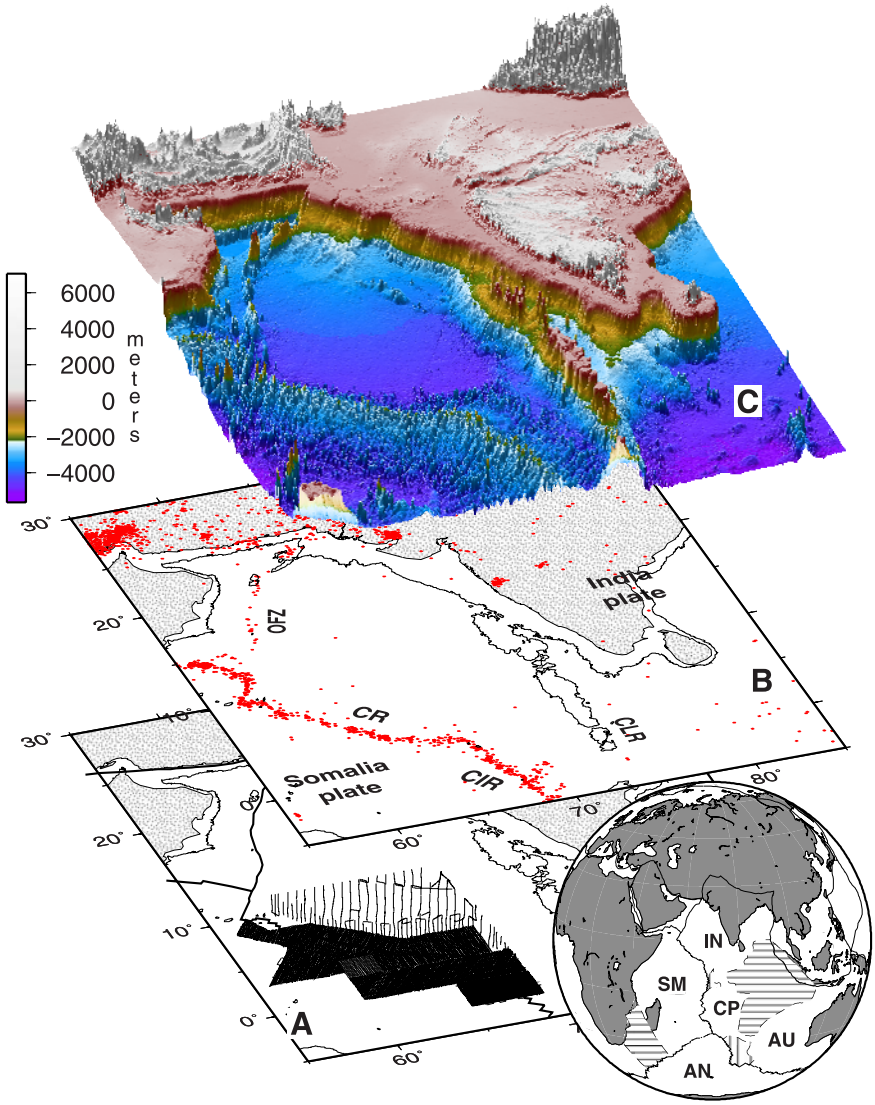

Figure 1. (a) Topography and bathymetry. (b) Seismicity and geography. (c) Tracks of the Russian shipboard magnetic data used in this study. Illuminated topography and bathymetry are from *Sandwell and Smith* [1997]. Inset globe at lower right shows the regional plate tectonic setting. Abbreviations: AN, Antarctic plate; AU, Australia plate; CP, Capricorn plate; CR, Carlsberg Ridge; CLR, Chagos-Laccadive ridge; IN, Indian plate; OFZ, Owen fracture zone; SM, Somalia plate.

rotations. We demonstrate that systematic errors in the anomaly crossings are comparable in magnitude to the random errors (sections 4.2 and 4.3), thereby implying that standard techniques significantly underestimate plate rotation uncertainties. To overcome this, we derive more realistic model uncertainties through data bootstrapping (section 4.4). We further modify the rotation uncertainties to account for likely and potential systematic biases in magnetic reversal and fracture zone locations (section 4.5). Readers who are interested principally in the kinematic analysis and tectonic implications should focus on results and discussion presented in sections 5–7.

2. Data

2.1. Marine Magnetics

[7] Our principal source of magnetic data consists of 236,000 kilometers of satellite-navigated Russian shipboard magnetics gathered during a series of systematic regional surveys in the 1980s (Figures 1 and 2) [*Karasik et al.*, 1986; *Glebovsky*

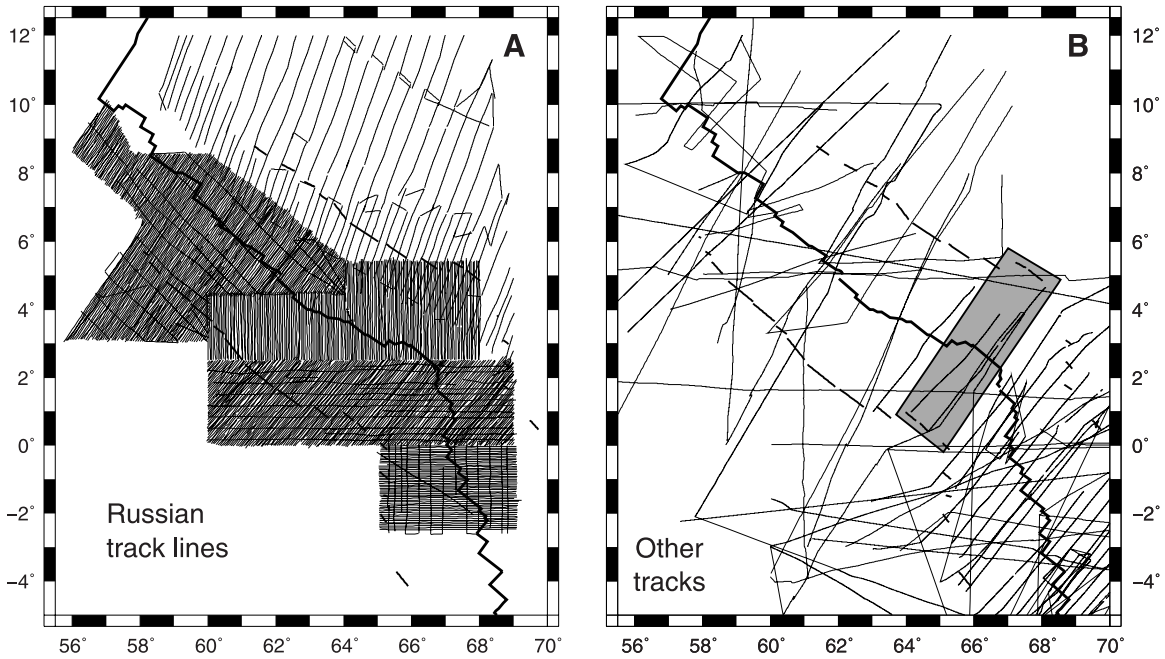

Figure 2. (a) Russian ship survey tracks. Magnetic grid derived from Russian data, and magnetic anomaly profiles are shown in Figure 3a. (b) Tracks of other shipboard and airborne magnetic profiles employed by *DeMets et al.* [2005]. Shaded region outlines region of magnetics highlighted in Figure 4. Bold lines flanking the ridge show positions of 20 Ma seafloor age isochrons.

et al., 1995; *Merkouriev and Sotchevanova*, 2003]. More than 90% of these data were collected along track lines that cross the Carlsberg and northern Central Indian ridges every ~5 km from 8.5°N to 2.5°S (Figures 1 and 2a), covering 1640 km of the plate boundary. These data cover seafloor out to ages of 20 Ma in most areas (Figure 2a). Additional dense surveys of even older seafloor south-

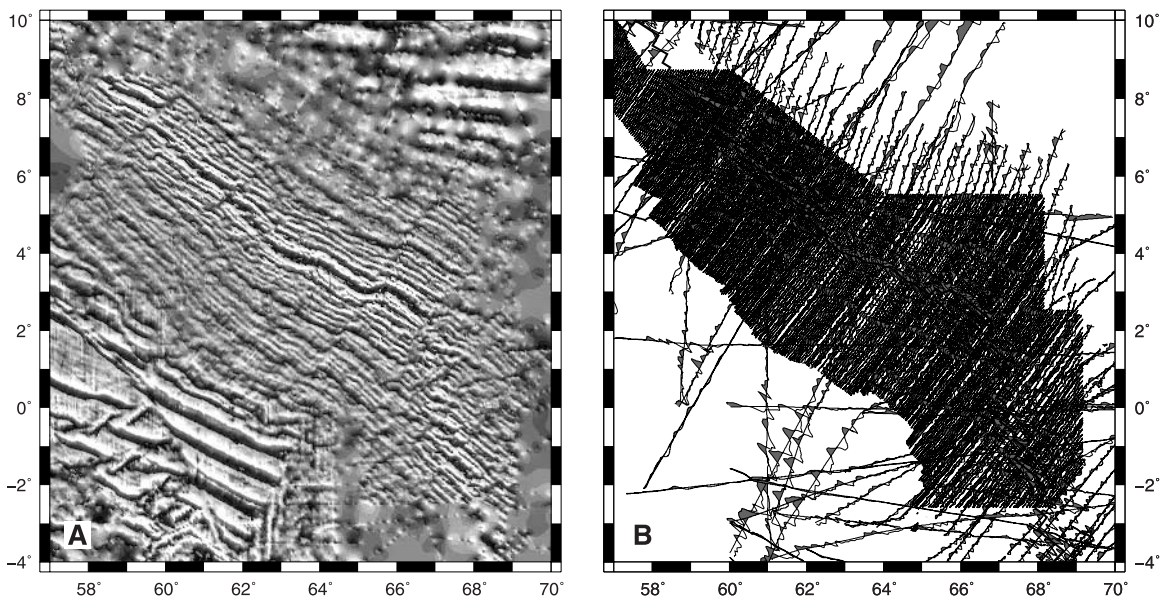

Figure 3. (a) Magnetic anomaly grid from Russian shipboard surveys. Illumination is from the northeast. (b) Magnetic anomaly profiles extracted from the Russian magnetic anomaly grid and other shipboard and airborne magnetic profiles.

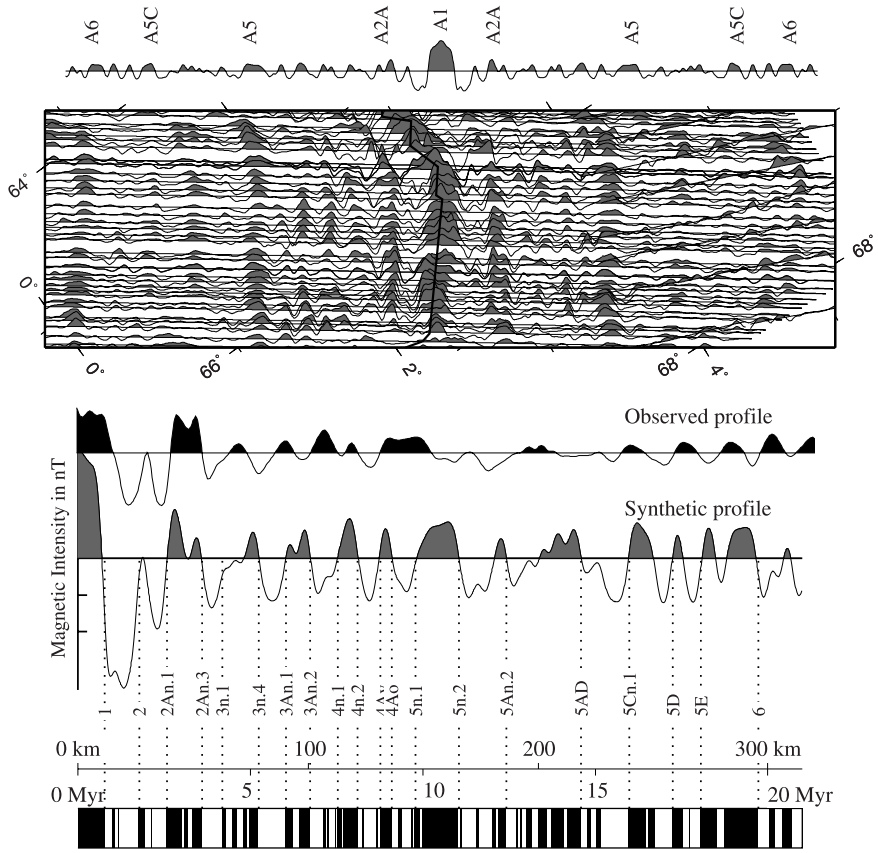

Figure 4. Close view of magnetic anomalies along Russian ship tracks from the shaded region shown in Figure 2. Projection is oblique Mercator using the best-fitting pole for C5n.2. Magnetic profile along the top edge of the map is a synthetic magnetic profile created assuming a full spreading rate of 29.5 km per Myr. The observed profile displayed below the map extends northeast from the ridge axis and is taken from the map. The one-sided synthetic magnetic anomaly profile below the map shows the assumed magnetic block model and correlation points (dotted lines) used for this study. A full spreading rate of 30 km Myr^{-1} and 1 km reversal zone transition width are employed. All profiles are reduced to the pole.

west of the Carlsberg ridge [*Glebovsky et al.*, 1995; *Merkouriev and Sotchevanova*, 2003] are not used for the ensuing analysis, although the magnetic anomaly grid displayed in Figure 3a incorporates these data.

[8] The original analog records from these surveys were digitized during the 1990s and were subsequently used by *Merkouriev and Sotchevanova* [2003] to create a magnetic anomaly grid (Figure 3a) that incorporates information from all Russian data within the survey region. The grid provides an outstanding view of the Vine-Mathews seafloor spreading lineations that flank the Carlsberg and northern Central Indian ridges, particularly northwest of 2.5°N, where few transform faults offset the ridge. We use this grid, which combines all of the information from the original surveys in an internally consistent and easy-to-use form, as the primary source of magnetic anomaly profiles for our analysis. We extracted 320 ridge-normal profiles from densely sampled portions of the grid, where original track spacings were only 5 km (Figure 3b). We used the original survey tracks as the basis for extracting data from the grid in areas where those tracks were approximately ridge-normal, thereby minimizing the use of interpolated anomaly intensities from areas of the grid located between the original survey tracks. The numerous extracted profiles (Figure 3b) sample the seafloor spreading lineations relatively uniformly at a spacing comparable to that of the original survey. Outside the densely surveyed regions, we used Russian data from more widely spaced (50–60 km) track lines on the Indian plate northeast of the ridge (Figure 2a), and American, British, French, and Indian shipboard magnetic and aeromagnetic observations compiled by DGR05 (Figure 2b).

[9] We reduced all magnetic profiles to the pole [*Schouten and McCamy*, 1972] to eliminate the nearly 180° phase shift that affects Carlsberg ridge

Table 1. Magnetic Anomaly Ages[a]

Chron	Age, Ma
C1o	0.781
C2y	1.778
C2An.1y	2.581
C2An.3o	3.596
C3n.1y	4.187
C3n.4o	5.235
C3An.1y	6.033
C3An.2o	6.733
C4n.1y	7.528
C4n.2o	8.108
C4Ay	8.769
C4Ao	9.098
C5n.1y	9.779
C5n.2o	11.040
C5An.2o	12.415
C5ADo	14.581
C5Cn.1y	15.974
C5Dy	17.235
C5Ey	18.056
C6noy	19.722

[a] Ages are from *Lourens et al.* [2004]. Chron designators followed by a "y" or "o" indicate the young or old edge of the chron, respectively.

magnetic anomalies. Figure 4 shows an example of the phase-shifted profiles that cross a 130-km-long spreading segment from 65.5°E–66.5°E. The sequence of well-lineated anomalies exhibits all of the major and shorter polarity intervals that should be present at this opening rate (see also the single observed half-profile shown in Figure 4).

[10] We interpreted the magnetic anomalies using large-scale maps of the residual magnetics superimposed on the regional bathymetry. The anomaly sequences are surprisingly well defined given the slow spreading rates characteristic of this plate boundary (21–34 km Myr^{-1}). We were unable to interpret magnetic anomalies located northwest of 58°E, in an area where several closely spaced fracture zones offset the ridge and Russian survey lines cover only the southern side of the plate boundary (Figure 2a). Similarly, we could not uniquely identify anomalies 3n.4 to 4n.2 from 60°E–63°E, where propagating rifts and their off-axis traces disrupt the anomaly sequence.

[11] We correlated all identifiable crossings of the twenty polarity reversals displayed in Figure 4 and listed in Table 1, ranging in age from 0.78 Ma (the Brunhes/Matuyama reversal) to 19.7 Ma (the old edge of anomaly 6). The numerous anomaly crossings fully define the paleo-axial geometry (Figure 5), thereby removing any ambiguity about how to reconstruct groups of anomaly crossings from opposite sides of the ridge. On the basis of results reported by *DeMets et al.* [2005], we adopt Fracture zone H as the northwestern limit of the diffuse India-Somalia-Capricorn triple junction and hence the geographic limit for anomaly crossings that are useful for constraining India-Somalia motion.

[12] Overall, we identified 6652 anomaly crossings (Figure 5), of which 6184 (93%) are from Russian data and the remaining 468 are from American, British, French, and Indian data. For a given rotation, as few as 241 and as many as 475 anomaly crossings are available to constrain motion (Table 2). These exceed by an order of magnitude or more the data that were used for previous studies of Carlsberg Ridge kinematics. For example, *Molnar et al.* [1988] use only 11 data (crossings of Anomaly 5) to characterize post-20 Ma seafloor spreading across the Carlsberg Ridge, fewer by a factor of 600 than the data used here. *DeMets et al.* [2005] use an average of 34 anomaly crossings for each of twenty reversals to estimate India-Somalia motion, most clustered along the northern Central Indian ridge. The sparse data available to them from the Carlsberg ridge frequently left gaps of 100 km and occasionally 200 km between adjacent anomaly crossings, thereby increasing the probability of mismatching isolated anomaly crossings from opposite sides of the ridge.

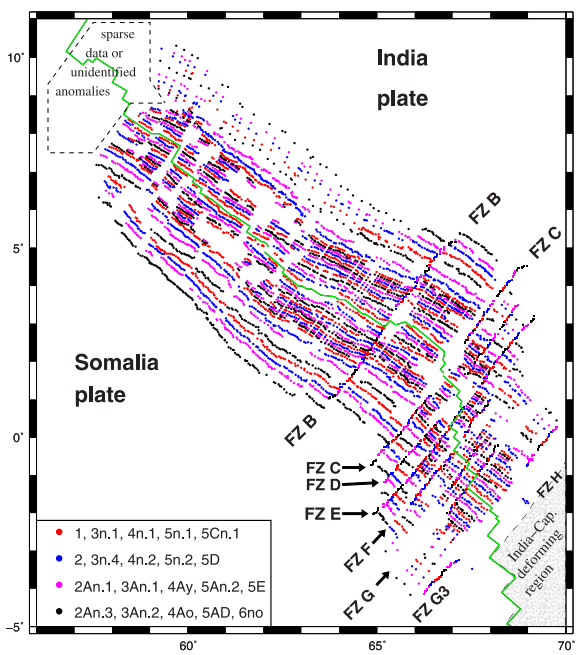

Figure 5. Crossings of magnetic anomalies and fracture zones used to determine India-Somalia motion. Magnetic correlation points are shown in Figure 4.

Table 2. India-Somalia Data Summary[a]

Chron	India-Somalia			
	N_{anom}	m_{anom}	N_{fz}	m_{fz}
1	345	24	56	4
2	361	20	57	4
2An.1	432	27	54	4
2An.3	365	20	85	7
3n.1	314	26	82	7
3n.4	337	19	85	6
3An.1	272	19	78	6
3An.2	271	18	78	6
4n.1	241	18	69	5
4n.2	293	20	69	5
4Ay	291	24	73	5
4Ao	306	21	69	5
5n.1y	375	22	65	5
5n.2	475	25	76	6
5An.2	390	24	69	5
5AD	308	19	72	5
5Cn.1	360	24	70	5
5D	338	20	70	5
5E	295	16	72	5
6no	283	18	45	3

[a] N_{anom} and N_{fz} are the numbers of magnetic anomaly and fracture zone crossings, respectively, that are used to constrain finite rotations for a given time. m_{anom} and m_{fz} are the respective numbers of paleo-spreading and paleo-transform segments used to define the paleo-plate boundary.

2.2. Fracture Zone Crossings

[13] Fracture zones B-G3, which offset the Carlsberg ridge east of 65°E (Figure 5), are mapped well enough to provide useful information about India-Somalia paleo-slip directions. Employing procedures described by DGR05, we systematically extracted crossings of these fracture zone valleys from a 2-minute bathymetric grid derived from the Russian bathymetric measurements and satellite altimetry (A. Briais, personal communication, 2004). Subsets of these crossings were selected to constrain paleo-slip directions for each of the twenty reversals listed in Table 1. In total, we use 1394 fracture zone crossings, the specifics of which are given in Table 2.

3. Analysis Techniques and Assumptions

3.1. Estimating Total Rotations

[14] We derive the rotations that best reconstruct magnetic anomaly and fracture zones from the India plate onto Somalia using the fitting criterion of *Hellinger* [1979]. For a paleo-plate boundary

Table 3. India-Somalia Finite Rotations and Covariances[a]

Chron	DOF	Lat., °N	Long., °E	Ω, degrees	Covariances					
					a	b	c	d	e	f
1	342	19.04	27.94	0.349	273.6	364.3	−50.2	767.6	84.7	171.5
2	367	21.78	30.86	0.754	84.8	47.0	−42.3	139.8	29.7	107.2
2An.1	421	22.90	30.60	1.068	391.7	422.5	−169.6	799.7	9.9	260.0
2An.3	393	19.58	33.72	1.594	341.4	380.6	−134.7	772.4	52.9	253.0
3n.1	327	21.75	28.44	1.745	657.9	801.8	−259.6	1398.9	−70.3	341.3
3n.4	369	22.10	31.62	2.179	263.4	343.8	−64.1	720.2	34.9	136.2
3An.1	297	21.96	29.30	2.406	4489.4	373.5	−5936.0	1117.7	257.8	8473.8
3An.2	298	21.28	30.90	2.748	290.0	418.8	−60.1	855.9	28.0	137.0
4n.1	261	22.55	30.55	2.982	624.2	1073.9	−107.7	2382.9	106.5	270.5
4n.2	309	21.97	30.83	3.285	582.1	895.8	−177.0	1727.1	−113.0	208.0
4Ay	303	22.41	30.75	3.489	546.8	607.1	−253.3	1297.9	89.6	428.5
4Ao	320	22.59	30.77	3.684	191.8	157.9	−105.1	374.7	43.6	197.6
5n.1y	383	23.57	30.46	3.888	374.5	494.6	−63.9	1053.5	154.0	232.0
5n.2	486	23.65	29.15	4.298	598.2	961.1	−30.9	2096.4	193.7	185.4
5An.2	398	23.72	29.22	4.878	592.3	563.6	−320.5	960.1	−36.7	431.0
5AD	329	24.59	29.15	5.761	409.9	686.1	−29.7	1439.8	58.2	104.5
5Cn.1	369	24.80	29.29	6.397	231.9	254.0	−88.8	614.9	24.6	139.9
5D	355	24.85	30.28	7.147	2430.6	1162.5	−2001.7	1013.8	−707.3	1854.6
5E	322	24.76	30.27	7.636	388.6	598.6	−59.7	1257.1	33.9	115.7
6no	283	25.98	30.69	8.430	8466.4	5974.7	−5804.5	8139.6	−1746.3	5532.2

[a] DOF is degrees of freedom, which equals the total anomaly and fracture zone crossings for a given chron minus twice the sum of the total number of segments and the number of rotation parameters (3). Rotations reconstruct the first plate relative to the second. Covariances are Cartesian and have units of 10^{-8} radians^2. Elements a, d, and f are the variances of the (0°N, 0°E), (0°N, 90°E), and 90°N components of the rotation. The covariance matrices are reconstructed as follows: $\begin{pmatrix} a & b & c \\ b & d & e \\ c & e & f \end{pmatrix}$

with p spreading and fracture zone segments, data from opposite sides of a seafloor spreading center are reconstructed using a trial rotation. The measure of misfit for a reconstructed segment is given by the summed, weighted, least-squares residual distances between the data along that segment and the great circle segment that best-fits those data. The measure of misfit for a trial rotation is thus the summed misfits for all p segments. A downhill simplex technique is used to identify the best-fitting rotation, with care taken to avoid local minima. Rotation uncertainties, expressed as covariance matrices, are estimated using methods described by *Chang* [1988] assuming Gaussian data noise. More realistic rotation covariances are estimated using techniques described in sections 4.4 and 4.5.

3.2. Orthogonal Rotation Component Plots

[15] For much of our analysis, we describe our kinematic results using rotation poles, opening angles, and seafloor spreading rates and directions, all of which are familiar to most readers. We also present our best-fitting plate rotations and their uncertainties in an alternative coordinate system whose three orthogonal component axes constitute a useful geometrically defined basis for understanding plate rotations and their uncertainties [*Stock and Molnar*, 1983; *Wilson*, 1993]. The first of these axes, coinciding with *Stock and Molnar*'s [1983] skewed-fit partial uncertainty rotation and Axis A of *Wilson* [1993], originates at the geocenter and points toward the geographic center of the India-Somalia plate boundary. A value of zero for the rotation component that parallels the skewed-fit axis indicates that the rotation lies 90° from this axis. Increasingly larger values for the skewed-fit rotation component correspond to increased fanning of magnetic lineations along the plate boundary and hence increasingly steep spreading rate gradients along the plate boundary.

[16] The second geometrically defined coordinate axis corresponds to the "mismatched magnetic anomaly" axis of *Stock and Molnar* [1983] and Axis B from *Wilson* [1993]. This axis is located 90° from the skewed fit axis along the great circle that contains both the best-fitting pole of rotation and the skewed-fit axis. The rotation component parallel to this axis describes the average opening angle along the plate boundary and is hereafter referred to as the pure-opening orthogonal component. The third axis is orthogonal to the first two axes and corresponds to the "mismatched fracture zones" axis of *Stock and Molnar* [1983] and Axis C of *Wilson* [1993]. The rotation component parallel to this axis contains information about the direction of slip along the plate boundary. We refer to it hereafter as the fracture-zone orthogonal component.

[17] These three geometrically defined axes typically lie close to the eigenvectors of the 3×3 rotation covariance matrix for a best-fitting rotation. Transforming the rotation covariances into the geometrically defined coordinate system is thus approximately equivalent to performing an eigendecomposition of the rotation covariance matrix. The diagonal terms of the transformed rotation covariance matrix are thus nearly the same as its eigenvalues, which by definition are uncorrelated and cleanly separate the constraints imposed by the data on the gradient in opening along the spreading axis, the average opening angle, and the opening direction.

[18] For a plate boundary that is characterized by constant opening, the magnitudes of the skewed-fit and pure opening orthogonal components extracted from a time series of rotations for that boundary will change linearly as a function of reversal age [*Wilson*, 1993], provided that reversal ages are perfectly known. Since they are not perfectly known, an alternative, more robust technique for detecting changes in motion is to examine the dimensionless ratio of these two component angles for a sequence of magnetic anomalies [*Wilson*, 1993]. This ratio will change only if seafloor spreading accelerates and/or the pole moves closer to or farther from the plate boundary. The fracture-zone component angle has a magnitude of zero for opening poles located along the great circle that connects the skewed-fit and pure opening axes, but acquires nonzero values if the plate slip direction changes and the pole hence deviates from this great circle.

4. Data and Model Uncertainties

[19] Sections 4.1–4.5 describe our efforts to estimate the magnitude of random and systematic errors in our data and quantify rotation uncertainties while accounting for both types of errors. The numerous data available for this work, consisting of hundreds of anomaly crossings from dozens of spreading segments for each of 20 polarity reversals (Table 2), make possible a strong test for the existence of systematic errors, one without precedent in the plate kinematic literature. Lacking

sufficient data to detect systematic errors, the authors of previous kinematic studies use a variety of techniques for estimating rotation uncertainties. Most assume that errors in the locations of anomaly crossings are predominantly random and Gaussian, thereby allowing them to estimate rotation certainties by propagating suitably scaled data uncertainties into the model covariances. This approach can significantly underestimate the uncertainties if there are unrecognized systematic errors in the data. Alternatively, some authors employ a more conservative approach to estimating rotation uncertainties by assuming that the true data errors significantly exceed those that are indicated by the data dispersion [e.g., *Stock and Molnar*, 1983].

[20] Random errors in magnetic anomaly locations can result from numerous factors such as errors in shipboard and airborne navigation, unmodeled temporal variations in the ambient magnetic field, unmodeled seafloor topography, and variations in the intensity of seafloor magnetization along the length of a magnetic lineation. Because these sources of error are typically uncorrelated between nearby magnetic profiles or decorrelate quickly along the strike of a magnetic lineation, they manifest themselves as random departures from a simple great-circle model for magnetic lineations. Numerous studies of plate motions have estimated the magnitude of these errors, which range from a few hundred meters to several kilometers [e.g., *Cande and Stock*, 2004; *DeMets and Wilson*, 1997; *Royer et al.*, 1997], depending on navigation quality and seafloor spreading rate. Random errors in our data are described in section 4.1.

[21] Systematic errors can be caused by a variety of processes, including small ridge jumps or offsets of the spreading axis by active or extinct propagating rifts, large seamounts, along-strike changes in the width of the reversal transition zone, and spreading rate-dependent variations in anomalous skewness [*Roest et al.*, 1992]. Such errors tend to systematically shift reversal locations closer to or farther from the ridge axis and typically affect the locations of reversals within a significant zone along the strike of a magnetic lineation, possibly including the entire spreading segment. Because it is unlikely that the processes described above will affect multiple segments in the same way, we refer hereafter to this type of error as ''segment-specific''. Such errors are difficult to detect unless a plate boundary consists of numerous well-surveyed segments for which reliable estimates of segment-specific average misfits can be determined. Segment-specific systematic errors in our data are described in section 4.2.

[22] A second, well-documented source of systematic error that affects plate opening estimates along entire plate boundaries is the displacement of magnetic reversal boundaries away from the axis of seafloor spreading due to the finite-width zone across which new seafloor accretes and records magnetic polarity transitions [e.g., *Sempere et al.*, 1987]. Extrusion of new magma onto adjacent older crust of opposite magnetization, intrusion of dikes into adjacent older crust of opposite magnetization, cooling and accumulation of magnetized gabbros at the base of the crust along a sloping reversal boundary, and extensional faulting of magnetic reversal boundaries all push reversal boundaries outward from the location they would occupy if reversals occurred and were recorded instantaneously [*Atwater and Mudie*, 1973]. Numerous in situ studies of magnetic polarity transitions on the seafloor indicate that reversal boundaries are displaced outward by 1–5 km with respect to their idealized locations [e.g., *Macdonald et al.*, 1983; *Sempere et al.*, 1987]. Boundary-wide systematic errors in our data are described in section 4.3.

4.1. Random Error: Dispersion Relative to Simple Great Circle Fits

[23] Following common practice, we define random errors in magnetic anomaly crossings using the dispersion of individual anomaly crossings with respect to a great circle segment that best fits data from that segment (section 3.1). To better estimate the magnitude of random errors, we determine individual best opening angles for each of the 424 spreading segments that define the India-Somalia plate boundary at the 20 times we selected (Table 1). By allowing for small differences in the closing angles for individual segments, segment-specific systematic errors are precluded from influencing the data misfit, as they would if a common opening angle for the whole boundary were enforced for a given time. There is too little information in magnetic anomaly crossings from a single spreading segment to constrain both the pole location and angle of opening for a given segment. For a given time and segment, we thus fixed the pole location to that of the best-fitting pole for that time (Table 3) and varied only the opening angle to minimize the data misfit.

[24] Figure 6a shows the residual distances of the 6652 anomaly crossings with respect to their best-

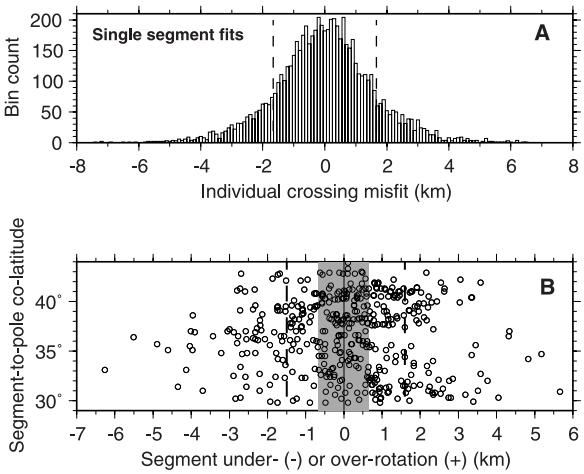

Figure 6. Data misfits. (a) Histogram of residual distances for fixed and rotated crossings of anomalies 1-6no relative to their best individual segment reconstructions (see text). (b) Overrotations and underrotations of the geographic centroids of rotated anomaly crossings with respect to fixed crossings per reconstructed segment for all twenty anomalies. Dashed lines in both panels show standard deviations of the misfits adjusted for the number of parameters used to fit the data. Shaded region in Figure 6b shows standard deviation of the misfits predicted by a Monte Carlo simulation for an idealized set of Carlsberg Ridge magnetic anomaly crossings perturbed by random location errors.

fitting great circle segments. Adjusting for the number of parameters used to fit the data, the standard deviation of the residuals is 1.67 km, constituting our best estimate of the random noise in the anomaly crossings. The 1394 fracture zone crossings have a standard deviation of 2.4 km for their residuals with respect to their individual best-fitting segment fits, constituting our best estimate of the random noise in the fracture zone crossings.

4.2. Segment-Specific Systematic Errors

[25] Segment-specific systematic misfits are estimated by inverting all data for a given time to estimate a best-fitting pole and opening angle and tabulating the average misfit for each segment from the resulting solution. For each segment, we determined a geographic centroid for data from the stationary plate and a centroid for data rotated from the opposite-side plate. We then determined the sense of misfit (overrotation or underrotation) between the centroids of the fixed and rotated data, and the distance between them measured along a small circle around the best-fitting pole.

[26] Figure 6b shows the distribution of the 424 segment-specific misfits for the 20 reversals we used in this study. Although the standard deviation of the residual distribution is 1.6 km, this does not necessarily represent the magnitude of segment-specific errors in our data because segment-specific misfits are attributable partly to random errors in the anomaly crossings, which will cause small segment-specific misfits even if there are no systematic errors in the data. We therefore estimate the effect of random errors in anomaly locations on the segment-specific misfits by using the Monte Carlo technique to determine the expected magnitude of segment-specific systematic misfits given a set of synthetic data whose geometry and random errors mimic those of our data.

[27] Using our best-fitting pole and opening angle, we first constructed a set of ideal anomaly crossings that mimic the geographic characteristics and number of data we use and have no errors. We next perturbed these idealized anomaly crossings with location errors drawn randomly from a Gaussian distribution with a standard deviation of 1.67 km, equivalent to the random noise observed in our data. Finally, we inverted the synthetic data to estimate a best-fitting rotation and tabulated the segment-specific misfits for each of the reconstructed segments. We repeated this procedure using 1000 different realizations of the randomly perturbed synthetic data to improve the reliability of our estimate of the expected systematic misfit.

[28] The resulting distribution of synthetically generated segment-specific misfits has a standard deviation of 0.66 km (shaded area in Figure 6b), defining the expected level of systematic misfit for magnetic anomaly crossings with random noise equivalent to that observed in our data. In contrast, the standard deviation for our observed segment-specific misfits is 1.6 km (dashed line in Figure 6b), significantly greater than expected for data with only random errors. We conclude that segment-specific systematic errors affect the anomaly crossings, and interpret the $\sim$1 km difference between the expected and observed standard deviations for the observed and synthetic segment-specific misfits as our best estimate of the magnitude of the segment-specific systematic error.

4.3. Boundary-Wide Systematic Error: Evidence for Outward Displacement

[29] Testing for systematic outward displacement of magnetic reversal boundaries along a plate boundary due to finite reversal transition zone widths is straightforward if spreading rates have been constant, as appears to have been the case for

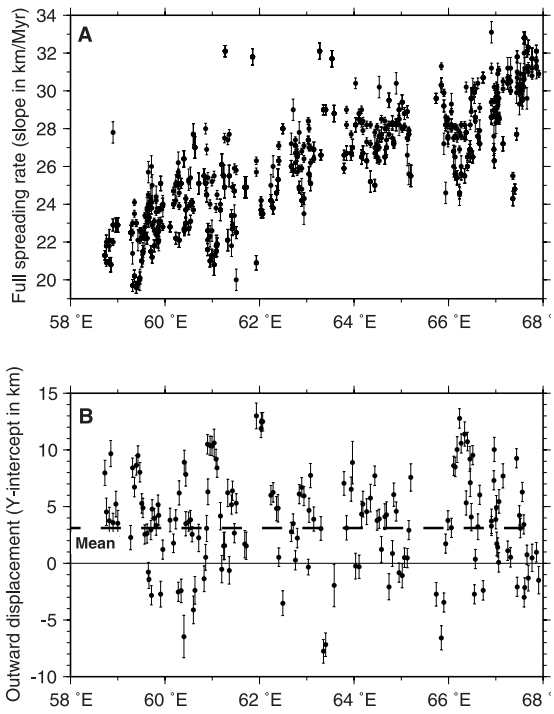

Figure 7. Results from linear regression of anomaly age versus total opening distances for 179 individual, flow-line-parallel magnetic profiles shown in Figure 3a. (a) Estimated opening rates (slopes) versus longitude along the Carlsberg ridge. (b) Best Y-intercepts. The strong bias of the y-intercepts toward positive values, with a mean bias of 3.1 km (dashed line), represents the well-known outward displacement of reversal boundaries from the axis of seafloor spreading due to the finite width of the zone in which new seafloor accretes.

India-Somalia seafloor spreading for at least the past 3.5 Myr [*DeMets et al.*, 2005]. If reversal boundaries are shifted systematically away from the spreading axis with respect to their idealized locations, linear regression of a time series of total opening distances for that spreading segment should yield a positive distance intercept for zero-age seafloor.

[30] We determined total opening distances versus magnetic reversal ages for 174 of the 320 ridge-normal magnetic profiles we extracted from the grid (Figure 3a), representing all profiles for which we were able to identify crossings of C1o, C2ny, C2An.1y, and C2An.3o on both sides of the spreading center. Figure 7 shows the opening rates (slopes) and distance-axis intercepts determined from linear regressions of the age-distance data for these 174 profiles. More than 80% of the distance-axis intercepts are positive, with a mean intercept value of 3.1 km. The boundaries of same-age reversals flanking the Carlsberg ridge are therefore shifted outward from the ridge by an average of 3.1 km more than expected given the observed opening rates. This falls within the 1–5 km range of in situ measurements of reversal transition zone widths [*Sempere et al.*, 1987].

[31] We also repeated the linear regressions described above for three alternative sets of reversals, drawn from the same 174 ridge-normal profiles, to determine whether the mean intercept value is sensitive to the set of reversals we selected for regression. One set of reversals consisted of C1o, C2y, and C2An.1y; the second consisted of all reversals through C3n.1y; and the third consisted of all reversals through C3n.4o. Regressions of these three alternative data sets yielded the same opening rates within uncertainties and respective mean distance intercepts of 2.6 km, 1.5 km, and 2.5 km. A positive value for the distance intercept is thus a robust outcome of the analysis. On the basis of the observed range of estimates (1.5–3.1 km), we assign a value of 2.5 ± 1 km for outward displacement along the India-Somalia boundary.

4.4. Realistic Model Uncertainties From Bootstrapping

[32] Although the technique described in section 3 for estimating best-fitting rotations and their uncertainties does not account for systematic errors in the data, it can be combined with the bootstrapping technique, which estimates best models via randomized resampling of the original observations [*Efron and Tibshirani*, 1986], to create a powerful alternative method for estimating best-fitting rotations and their uncertainties in the presence of random and systematic data errors. Implementation of the bootstrap technique to estimate a model from a set of N observations requires that N samples be drawn randomly from the original data. Each randomized sample is inverted to estimate a best model and the process is repeated many (thousands) times to generate a large number of alternative models. The frequency with which a particular observation is randomly selected during a given run determines its weighting relative to other data. The technique thus effectively explores the influence of randomized alternative data weighting schemes on the model. For data with systematic errors or poorly known uncertainties, bootstrapping explores a wide range of potential

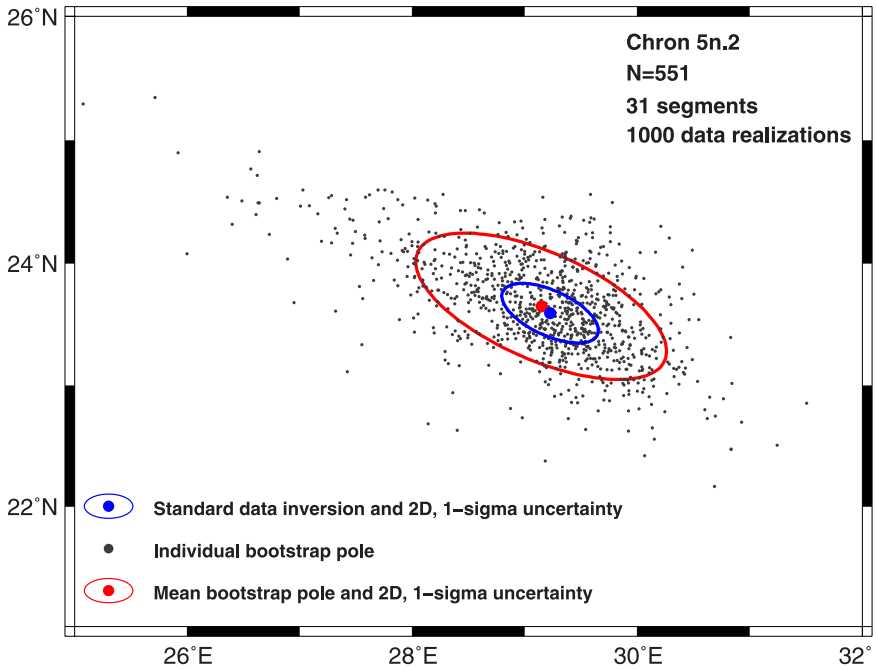

Figure 8. Formal (blue ellipse) and bootstrapped (red ellipse) pole confidence limits for Chron 5n.2. Individual bootstrap pole locations best fit 1000 independent realizations of the Chron 5n.2 data set, each consisting of 31 randomly selected spreading and fracture zone segments that equal in number the 31 segments into which the 551 magnetic anomaly and fracture zone crossings for Chron 5n.2 are subdivided (Figure 5). The larger bootstrapped confidence limits indicate that the formal uncertainties propagated from the assumed random noise in the data locations understate the actual uncertainties, most likely due to nonnegligible intrasegment systematic errors that are not accounted for in the formal uncertainty estimate.

models and hence can be used to derive more realistic model uncertainties.

[33] Since our goal is to better account for the effect of segment-specific systematic data errors on our best-fitting rotations and their uncertainties, we selected and inverted all data from M randomly selected segments from the India-Somalia spreading center for a given reversal and trial model. Individual anomaly crossings were uniformly assigned unit weights. Data from a segment that was randomly selected N times for a particular trial run were thus weighted a factor of $\sqrt{N}$ greater than their unit weight, thereby systematically altering the weight of all data from that segment relative to data from other segments.

[34] Figure 8 shows the outcome of this procedure for 1000 random resamplings of the 31 segments into which the 551 C5n.2 anomaly and fracture zone crossings are grouped. The 1000 best-fitting bootstrap poles are centered on a mean pole that differs insignificantly from the pole that best-fits the original 551 C5n.2 data. The rotation covariance matrix that best describes the 3-dimensional distribution of 1000 bootstrapped rotations with respect to the best-fitting rotation is derived from a 3×3 orientation matrix [*Fisher et al.*, 1993]. The semimajor and semiminor axes of the 2D, 1-σ confidence ellipse extracted from the bootstrap-derived covariance matrix (red ellipse in Figure 8) are a factor of two or more larger than those for the formal confidence ellipse (blue), which is derived assuming that all data errors are random and Gaussian-distributed. The difference in the sizes of these alternative confidence ellipses demonstrates that systematic errors contribute significantly to the overall model uncertainty and thus cannot be ignored. The same pattern is true for all twenty reversals; the bootstrapped confidence regions are always significantly larger than the formal error estimates.

4.5. Additional Systematic Errors

[35] Two additional sources of systematic error affect the data and thus merit incorporation into the rotation covariances. The first is the limited precision with which reversals can be identified at slow spreading rates for closely spaced magnetic polarity intervals. For example, the irregular sloping shape of the young edge of the anomaly 3 sequence, which consists of four relatively short

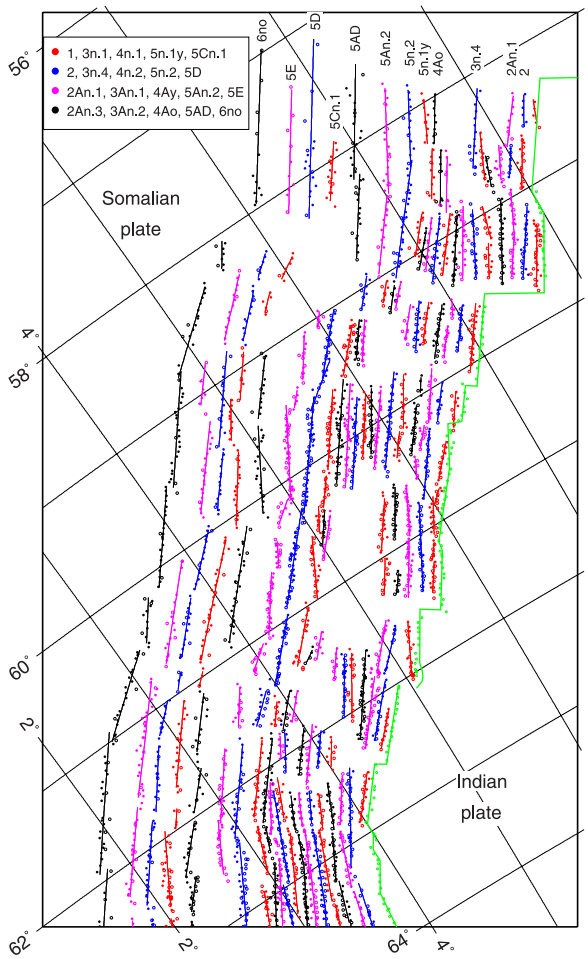

Figure 9. Best-fitting reconstruction of Carlsberg Ridge magnetic anomaly and fracture zone crossings onto Somalia plate. Projection is oblique Mercator centered on 22°N, 30.5°E. Figure is drawn to same scale as Figure 10.

polarity intervals (Figure 4), makes it difficult to identify the precise location of C3n.1y. Similarly, interference from the brief anomaly 3B sequence at the young edge of C4n.1 adds uncertainty to the precise definition of the young edge of C4n.1. We estimate that the precision with which we can identify the location of any particular magnetic reversal is limited to ±0.5–1 km, depending on the particulars of the waveform for each reversal. A systematic mispick of the location of a given reversal everywhere along the plate boundary is equivalent to introducing a systematic error into the angle of rotation. To account for this potential source of systematic error, we conservatively added the angular equivalent of ±1.0 km to our best-fitting rotation covariances, as described below.

[36] We are similarly limited in our ability to identify the precise location of paleoslip within a fracture zone valley. Lacking multibeam surveys of any of the fracture zones that record India-Somalia motion, we assume that paleoslip is focused in the deepest part of a fracture zone valley. Given that paleoslip within the valley may not have coincided with its present bathymetric maximum and could moreover have varied with time, we subjectively incorporate an additional ±2 km of systematic error directed perpendicular to the fracture zone segments.

[37] We incorporated these additional uncertainties into the rotation covariances as follows: We first transformed the covariance matrix for each reversal into the geometrically defined coordinate system described in section 3.2. We then added the angular variances associated with the uncertainties in identifying reversal locations and locations of paleoslip to the variances associated with the pure-opening and fracture-zone orthogonal components, respectively. Finally, we transformed these modified covariances back to their geocentrically based coordinate system. The modified covariance matrices (Table 3) represent our best estimate of the rotation uncertainties.

5. Results: Best-fitting Rotations and Uncertainties

[38] Employing procedures and results described in sections 3.1, 4.4, and 4.5, we derived best-fitting rotations and uncertainties for all twenty reversals we studied (Table 3). Uniform uncertainties of 1.7 km and 2.4 km were assigned to all anomaly and fracture zone crossings, reflecting their respective random dispersions with respect to simple great circle fits. The best-fitting rotations represent the mean value of the 1000 best-fitting bootstrap rotations for each polarity reversal.

5.1. Reconstructed Plate Geometry

[39] Figures 9 and 10 show the best reconstructions of Indian plate data onto the Somalia plate using the best-fitting rotations (Table 3). To first order, the ridge-transform geometry has been stable since 20 Ma. A comparison of opening distances from the ridge axis out to C6no everywhere along the plate boundary reveals no evidence for spreading asymmetries that exceed 5%, in accord with the absence of evidence for significant changes through time in the paleo-axial offsets of fracture zones B-G. The azimuths of reconstructed

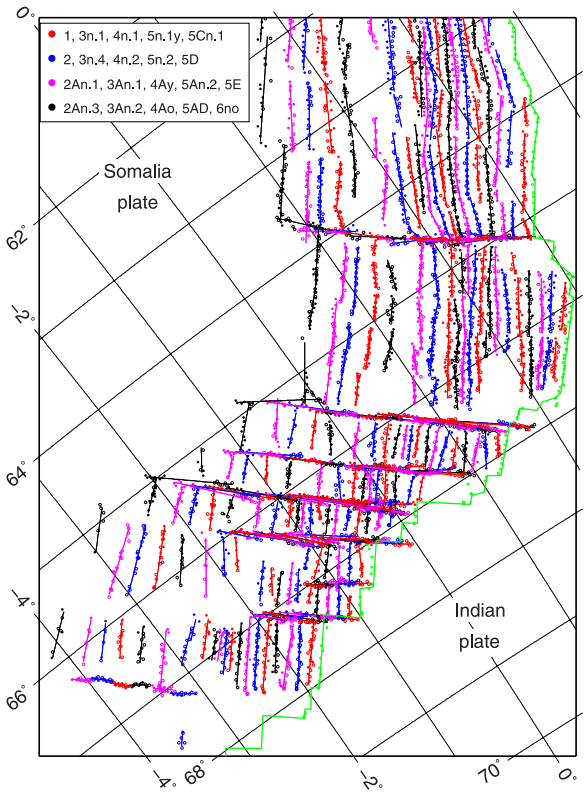

Figure 10. Best-fitting reconstruction of northern Central Indian Ridge and southeastern Carlsberg Ridge magnetic anomaly and fracture zone crossings onto Somalia plate. Projection is oblique Mercator centered on 22°N, 30.5°E. Figure is drawn to same scale as Figure 9.

magnetic lineations and fracture zone segments also have changed by no more than ~10° since 20 Ma (Figure 11), consistent with a stable plate boundary geometry.

5.2. Pole Locations

[40] Our best-fitting rotation poles (Figure 12) form a consistent time series, with poles for successively younger anomalies located within each other's 2-D, 1σ confidence ellipses. Only the C2An.3 pole lies significantly outside the error ellipses of the next youngest (C2) and oldest (C3n.1) rotations. Although we suspect that the anomalous C2An.3 pole is caused by a data-related problem such as miscorrelated magnetic anomalies for one or more spreading segments, inversions of different subsets of the C2An.3 data to determine which (if any) subset of the data is problematic reveals no obvious problem with any of the data. Nonetheless, it seems unlikely that the anomalous C2An.3 pole represents evidence for a temporary change in plate motion given the strong evidence described below for steady India-Somalia motion for the past 9–10 Ma.

[41] Relative to the India-Somalia poles from DGR05, which also describe motion since 20 Ma, the newly derived best-fitting poles define a more tightly clustered and hence simpler pattern. For example, six of the 20 poles reported by DGR05 are located more than four angular degrees from the centroid of their pole distribution, whereas only two of the 20 poles derived here are located more than four angular degrees from their central location.

5.3. Seafloor Spreading Rates

[42] Figure 13 shows the evolution of post-20 Ma seafloor spreading rates at a centrally located point along the India-Somalia boundary. The interval rates and their uncertainties are determined using stage rotations and covariances derived from the best-fitting finite rotations and their covariances (Table 3). *Lourens et al.* [2004] estimate that uncertainties in the ages of reversals younger than 12.4 Myr are ±0.01–0.02 Myr, too small to alter significantly the rate uncertainties we propagated

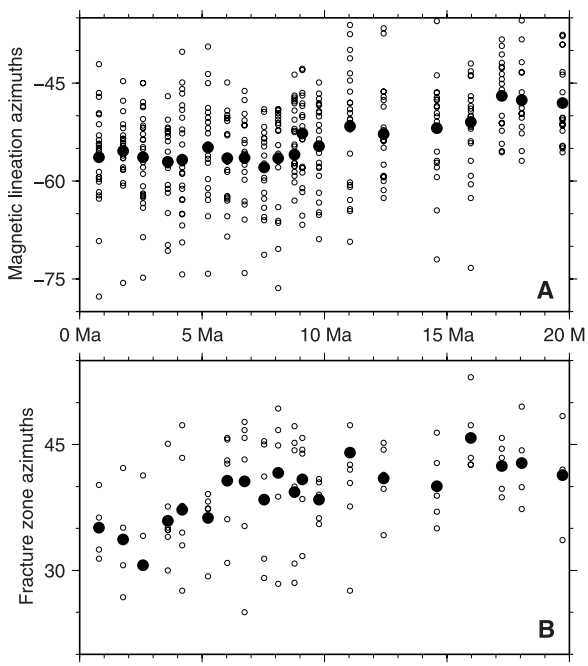

Figure 11. (a) Time evolution of reconstructed magnetic lineation azimuths in degrees CW of N. (b) Time evolution of reconstructed fracture zone segment azimuths. Small open circles in both panels show best-fitting azimuths to individual reconstructed magnetic lineation or fracture zone segments from Figures 9 and 10. Filled circles show mean directions determined from the individual azimuths.

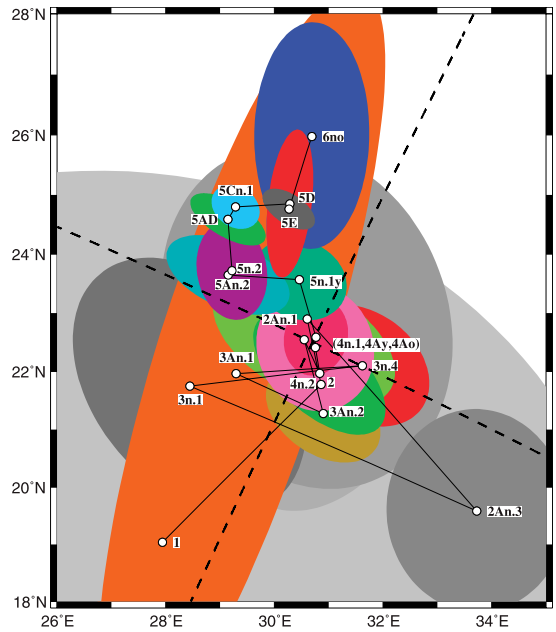

Figure 12. India-Somalia finite rotation poles and 2-D, 1-sigma confidence regions derived from covariances modified using bootstrapped procedure and incorporating estimated systematic errors, as described in the text. Dashed lines show great circles along which changes in pole location depicted in Figure 16 are calculated.

from our already conservative rotation covariances. Uncertainties in the ages of reversal older than 12.4 Myr are difficult to estimate and are discussed explicitly in the analysis below. Uncertainties in the astronomically calibrated reversal ages are not propagated into the stage rate uncertainties.

[43] Interval spreading rates from 20 Ma to 10 Ma decelerated ~30%, from 42 ± 2 mm yr^{-1} before 16 Ma to rates of 30 ± 1 mm yr^{-1} at 10 Ma (Figure 13). The 30% rate slowdown from 20–10 Ma might be an artifact of errors in the ages of reversals older than 12.4 Ma, some of which lack the same degree of astronomical age calibration as do younger reversals [*Lourens et al.*, 2004]. However, for reasons described below, it seems improbable that errors in the ages of the older reversals are combining in a way that fortuitously yields a rate slowdown. For example, spreading rates from C5An.2o (12.415 Ma) to C5Cn.1y (15.974 Ma), whose ages are both astronomically calibrated, averaged 34 ± 1 mm yr^{-1}, significantly faster than the opening rate since ~10 Ma. Similarly, the 37 ± 1 mm yr^{-1} opening rate for the period from 19.7 Ma to 11 Ma (C6no-C5n.2) exceeds by 23% the 0–10 Ma opening rate. The small uncertainty in the astronomically calibrated age for C5n.2 (±0.01–0.02 Myr) adds almost no uncertainty to the stage opening rate determined for this 8.7-Myr-long interval. As a consequence, C6no would have to be 2.0 Myr older than the age assigned by *Lourens et al.* [2004] in order to yield a C6no-C5n.2 interval rate as slow as the 30 mm yr^{-1} 0–10 Myr opening rate. Such a large adjustment in the estimated age of C6no would require an implausibly large adjustment of the well-determined, astronomically tuned 23.0 Ma age for C6Cn.2 estimated by *Lourens et al.* [2004].

5.4. Orthogonal Rotation Components

[44] A comparison of the orthogonal rotation component angles and their uncertainties for the new rotations and those from DGR05 emphasizes the positive impact of the numerous new data on the accuracy and precision of our India-Somalia estimates (Figure 14). The DGR05 orthogonal rotation components exhibit significantly more scatter than do the new estimates. For example, linear regressions of the skewed-fit and pure opening component angle pairs (Figure 14a) for the new and DGR05 models using unit weighting for all angles yields a least-squares misfit χ^2 for the new model that is a factor of four smaller than for the DGR05 model. The average misfit of a simple constant motion model to the new component angles is thus only half as large as the average misfit for the DGR05 component angles. The new data are thus more consistent with a simpler model for post-20 Ma opening.

[45] The uncertainties in the newly derived rotations are also significantly smaller than reported by DGR05 despite our more conservative technique for estimating rotation uncertainties. The bootstrapping and covariance-modification procedures that we employ to estimate rotation uncertainties yield uncertainties that are on average a factor of two or more larger than the formal errors we would have derived if we had employed procedures identical to those used by DGR05. That the uncertainties in Ω_{skew}, shown by the vertical components of the uncertainty ellipses in Figure 14a, are typically reduced by factors of 2–5 relative to those for the DGR05 study is strong evidence that the large number of anomaly crossings we use have significantly improved our description of India-Somalia motion.

6. Testing for Changes in India-Somalia Motion

[46] The central question of our kinematic analysis is whether seafloor spreading between India

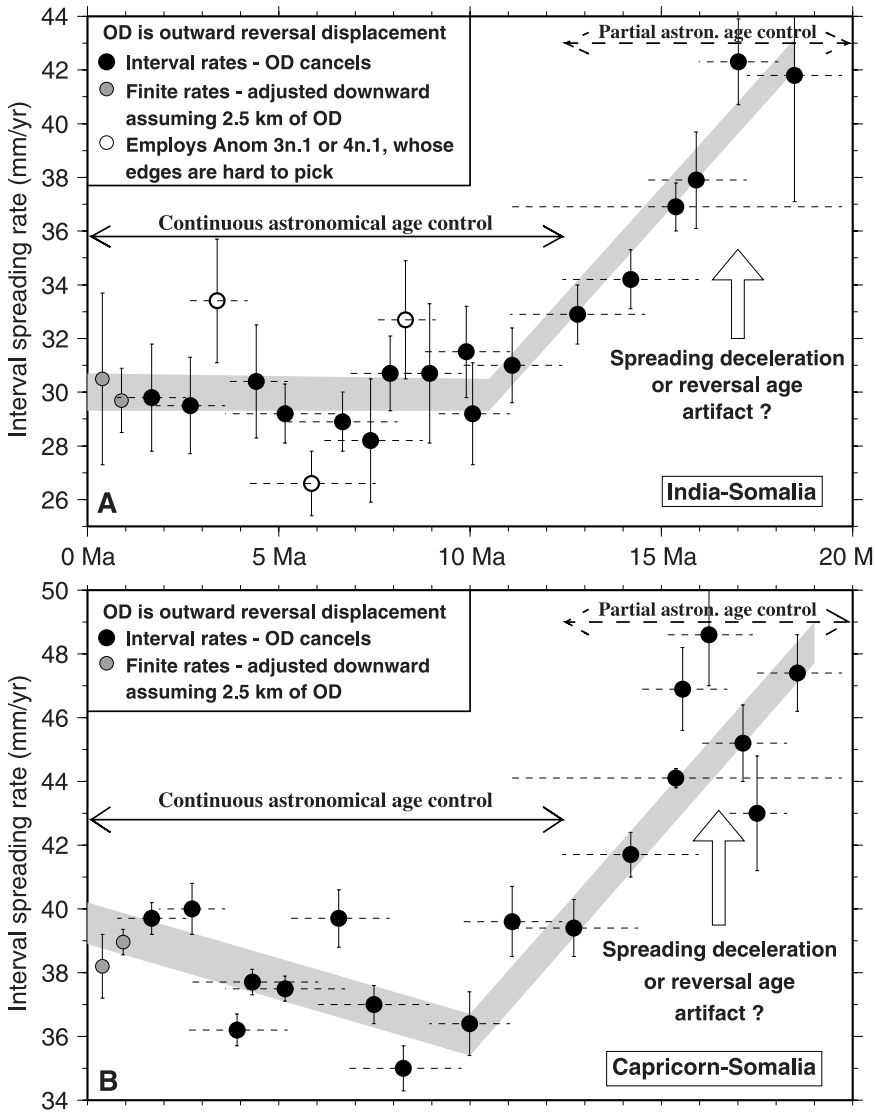

Figure 13. (a) India-Somalia interval spreading rates. (b) Capricorn-Somalia interval spreading rates. The stage rotations and covariances that are used to calculate the interval rates and their standard errors are derived from India-Somalia finite rotations and covariances (Table 3) and Table 3 of *DeMets et al.* [2005] for Capricorn-Somalia. Dashed horizontal lines indicate the time interval over which motion is averaged. Shaded bands indicate schematic interpretations of the spreading history. Assumed reversal ages are given in Table 1.

and Somalia changed significantly since 20 Ma, possibly in concert with the well documented change in Capricorn-Somalia motion at 8 ± 1 Ma [*DeMets et al.*, 2005]. Sections 6.1–6.3 describe a series of tests designed to answer this question rigorously. We first test for changes in the India-Somalia pole location, which determines the seafloor spreading gradient and spreading direction, and then test for evidence of significant changes in seafloor spreading rates. Finally, we undertake a rigorous test for motion changes that employs orthogonal rotation components and their full uncertainties.

6.1. Changes in Pole Location

[47] We begin by testing whether our kinematic data are consistent with the hypothesis that the India-Somalia pole has remained stationary for some or possibly all of the past 20 Myr. Following procedures outlined in DGR05, we test this hypothesis for a series of progressively longer inter-

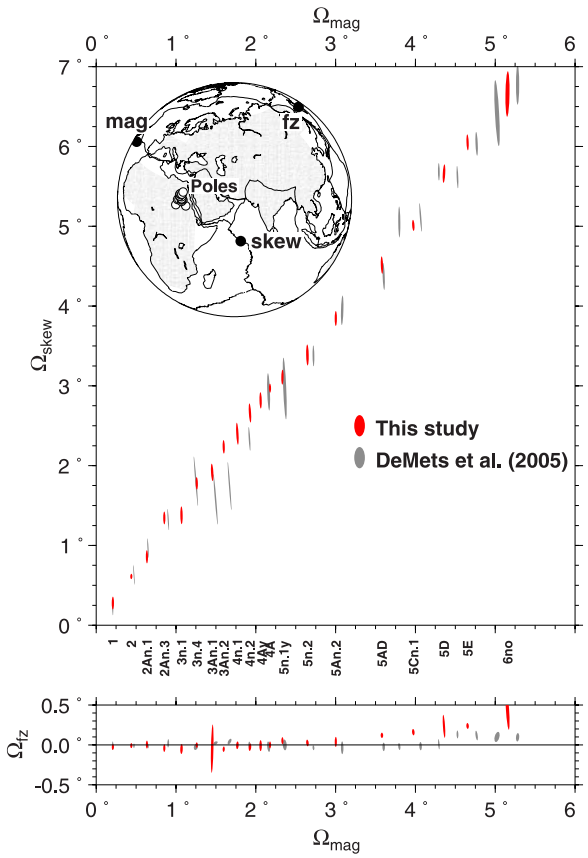

Figure 14. Orthogonal component plot of India-Somalia rotations and 2-D 1-sigma error ellipses derived using bootstrapped procedure and incorporating estimated systematic errors, as described in the text. Results from *DeMets et al.* [2005], derived from an order-of-magnitude fewer data, are shown for comparison. Open circles on the inset globe show pole locations from Figure 12. Ω_{skew}, Ω_{mag}, and Ω_{fz} are the respective components of the rotations along the approximate locations of the skew-misfit, magnetic-anomaly misfit, and fracture-zone misfit eigenvectors, the locations of which are shown on the inset globe.

vals, beginning with 0–3 Ma and ending with 0–20 Ma. For a given interval, spanning N reversals, we assume that the best stationary pole coincides with the Fisher mean location of the N best-fitting poles within that interval, each weighted by its respective opening angle. For each of the N reversals, we invert the magnetic anomaly and fracture zone data to estimate the best opening angle for the stationary pole. We then compare the summed least-squares misfit for all N reversals to the misfit for their best-fitting rotations (Table 3), which do not impose a stationary pole assumption.

[48] Figure 15 illustrates the outcome of this test. For all intervals extending from the present back to 9–10 Ma, the differences in the fits of the stationary-pole model and best-fitting rotations remain approximately the same, indicating that a stationary pole assumption for the past 9–10 Ma does not force a significantly worse fit to the data than requiring a stationary pole for much shorter intervals (0–3 Ma for example). Although the differences in the fits of the stationary-pole and best-fitting models are statistically significant if measured with the F-ratio test, the existence of significant systematic errors in our data violates the Gaussian noise assumption that is implicit in the F-test. As an alternative measure of the significance of the misfit, we used the best-fitting and stationary-pole rotations for C4Ao (9.1 Ma) to predict total opening distances at the two ends of the plate boundary. The opening distances predicted by the two models differ by only 300 meters (0.1% of the total opening) at both ends of the plate boundary, less than the likely 1-km systematic errors in our data. We conclude that the data are consistent with a stationary India-Somalia pole for the past 10–9 Myr.

[49] For intervals longer than the past 9–10 Myr, the fits of the stationary pole models become progressively worse (Figure 15) than the best-fitting model fits. For the longest interval we can test, extending from the present to 19.7 Ma (C6n), the difference in the opening distances predicted by the stationary pole and best-fitting models is 2.5 km, comparable to or larger than the random and systematic errors characteristic of our data (sections 4.1–4.3). The data are thus inconsistent with a model in which the India-Somalia pole has remained stationary since the time of Chron 6.

[50] A visual inspection of the time sequence of best-fitting poles (Figure 12) exhibits the reason for the increasingly large misfits of the stationary pole models for periods before 9–10 Ma. The poles for reversals as old as 9.1 Ma (C4A) generally fall within each other's error ellipses and show no consistent pattern of pole migration. In contrast, poles for older reversals are located several angular degrees to the north and exhibit a time-progressive southward migration toward the cluster of poles associated with reversals younger than C5n.1.

[51] The observed migration of the opening pole from its position prior to ~10 Ma to its post-10 Ma position brought it 2.5° closer to the plate boundary (Figure 16). This increased the gradient in the spreading rate along the length of the India-Somalia boundary by 0.6 mm yr^{-1} per 1000 km of ridge length, approximately 2% of the total opening rate.

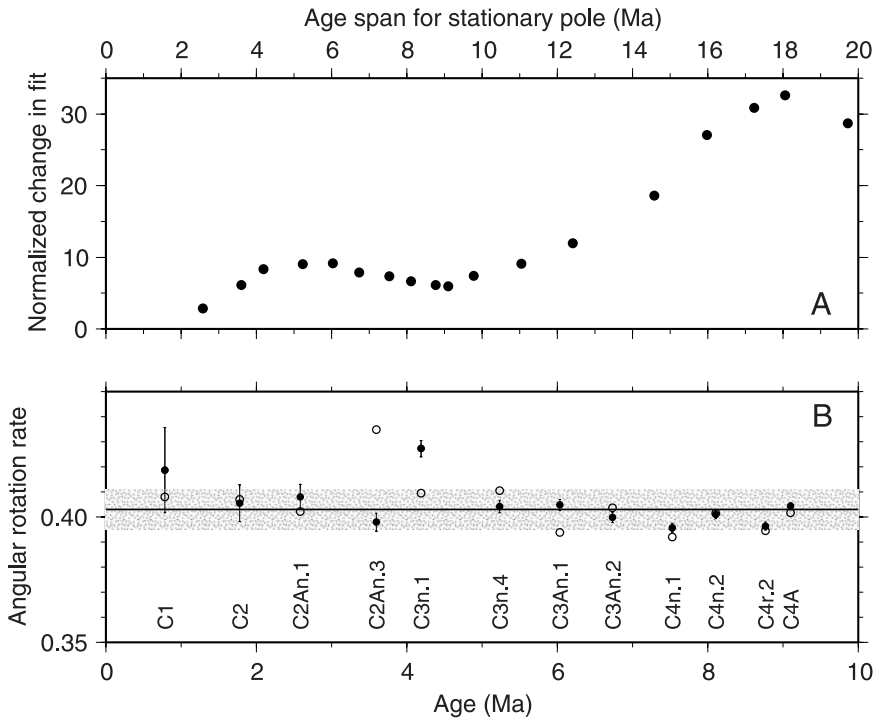

Figure 15. Test for stationary pole and angular rotation rate. (a) Change in the least-squares fit to anomaly and fracture zone crossings for periods from present back to a given time for two models. Model 1 assumes the pole has remained fixed at a central location from the present back to a given time and adjusts only the opening angles to optimize the fit to the data. Model 2 employs separate best-fitting rotations to optimize the fit to data (Table 3). Vertical axis shows the Model 2 least-squares fit subtracted from that for Model 1, normalized by the number of additional rotation parameters used to fit the data for Model 1 versus Model 2. (b) Best rates of angular opening for Model 1 (solid circles) and Model 2 (open circles). All opening angles are adjusted downward to correct for 2.5 km of outward displacement (section 4.3) and are divided by their assumed reversal age (Table 1). Shaded region indicates variation of ±2% above and below the mean rate. Error bars are 1-sigma and include assumed uncertainties of ±10,000 years [*Lourens et al.*, 2004] in reversal age estimates and ±1 km for the correction for outward displacement.

The southward pole migration also resulted in a 5–10° counterclockwise shift in the opening direction that is exhibited by both the magnetic lineations and fracture zone segments (Figure 11). Within errors, the change in pole location appears to have started no earlier than 11 Ma and ended no later than 9 Ma (Figure 16).

6.2. Changes in Angular Opening Rates Since 10 Ma

[52] In light of the evidence presented above that both the opening pole and interval spreading rates have been steady since 9–10 Ma, we tested whether our data are consistent with a constant rate of angular opening during this period. Figure 15b shows the sequence of angular velocities that we derived by dividing the best-fitting opening angles associated with our stationary pole model for 0–9.1 Ma by their estimated reversal ages (Table 1). After adjusting all 12 opening angles downward to correct for 2.5 km of outward displacement (section 4.3), 10 of the 12 angular opening rates have values within 2% of the mean angular opening rate of 0.403° Myr^{-1}, and 11 of the 12 angular rates are consistent with the mean within their standard errors. Within their uncertainties, these independently derived angular opening rates are consistent with a remarkably steady angular opening rate since 9 Ma. We suspect that the only anomalous angular opening rate, that for C3n.1 (4.2 Ma), is caused by difficulty in accurately picking the precise location of the hard-to-define young edge of Anomaly 3.

[53] We conclude that within the uncertainties, the India-Africa pole has been fixed and its angular opening rate has changed less than 2% since 9–10 Ma. The pole that coincides with the Fisher mean location for the twelve best-fitting rotations for Chrons 1 through 4A(old) is located at 21.9°N, 30.7°E. The angular rotation rate most consistent with data is 0.403° Myr^{-1}, corresponding to a full spreading rate of 30.0 ± 0.6 mm yr^{-1} at the center of

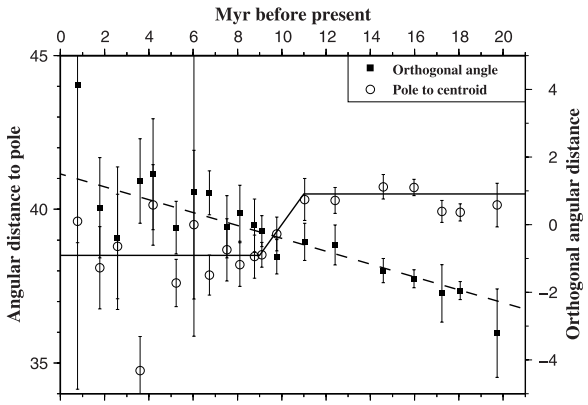

Figure 16. Changes in India-Somalia pole locations as a function of the reconstruction age. Open circles show angular distance from pole to the plate boundary along a great circle that connects the two (shown in Figure 12). Solid squares show angular distance of pole measured orthogonal to the same great circle. The circles thus show migration of the pole toward and away from the boundary, representing changes in the along-axis gradient in seafloor spreading. Boundary-orthogonal pole migration shown by the squares represents change in opening directions. Increasingly negative angles represent increasingly clockwise opening directions.

the plate boundary. These constitute our best estimate of India-Somalia motion for the past 10 Myr.

6.3. Orthogonal Component Analysis

[54] We next employ the pure opening, skewed-fit, and fracture zone component angles (section 3.2) to search rigorously for changes in India-Somalia motion since 20 Ma. Since our rotation covariance matrices incorporate the full set of known data errors and biases, a search for changes in plate motion that is based on the orthogonal rotation components and their uncertainties is a more conservative test for plate motion changes than was possible in sections 6.1 and 6.2.

[55] Guided by the results described above, we compare the fits of models in which motion is allowed to change once over the past 20 Ma against a model in which steady motion is enforced. To do this, we used linear regression of the component angle pairs to identify the line that minimizes the root-mean-square misfit, where the misfit for an individual component angle pair is measured in a direction orthogonal to the best-fitting line and is weighted by their combined uncertainties. All uncertainties in the component angles are extracted from their corresponding rotation covariance matrix (Table 3).

[56] For the pure opening versus skewed-fit component angles, a constant-motion model that allows for no changes in motion for the past 20 Ma misfits 13 of the 20 component angle pairs by more than their conservatively estimated standard errors (Figure 17a). Such a model can be rejected at a confidence level of 99.94% on the basis of its poor fit to the data. In contrast, models in which motion is assumed to have changed at 9.1 Ma (C4Ao) or even more recently improve the fit at the 95% confidence level (Figure 18a) relative to the fit of a constant motion model.

[57] For the pure opening versus fracture zone component angles (Figure 17b), a constant-motion model significantly misfits 12 of the 20 component angle pairs, indicating once again the inconsistency of the data with a constant motion model. Every two stage model we tested significantly improves the fit relative to the constant motion model (Figure 18b), with the best fit coinciding with an assumed change in motion at 6.7 Ma.

[58] The component angle data are thus fit significantly better by models that allow for a change in motion as early as 9 Ma or as recently as 5 Ma than by a constant motion model (Figures 18a and 18b), even allowing for our conservative estimates of the rotation uncertainties. The greatest improvement in the fit relative to the constant motion model occurs for angle pairs associated with reversals younger than 10 Ma (Figures 17b and 17d). None of the models fit component angles very well for reversals older than 10 Ma, even within their conservatively estimated uncertainties. The poor fit suggests that a constant motion model for motion before ~10 Ma may not be applicable, as suggested by the evidence for a gradual spreading slowdown from 20–10 Ma (Figure 16).

7. Discussion

7.1. Comparison to DGR05 Results

[59] On the basis of many fewer magnetic anomaly and fracture zone crossings from the Carlsberg and northern Central Indian ridges, *DeMets et al.* [2005] conclude that motion between India and Somalia has been constant for the past 20 Ma. Although we concur that motion has been constant for at least part of this time, we find evidence for the following significant changes: (1) India-Somalia seafloor spreading rates slowed down by ~30% from 20–9 Ma (Figure 13), (2) The pole shifted location at 11–9 Ma, including a 3° shift toward the plate boundary that increased the gradient in

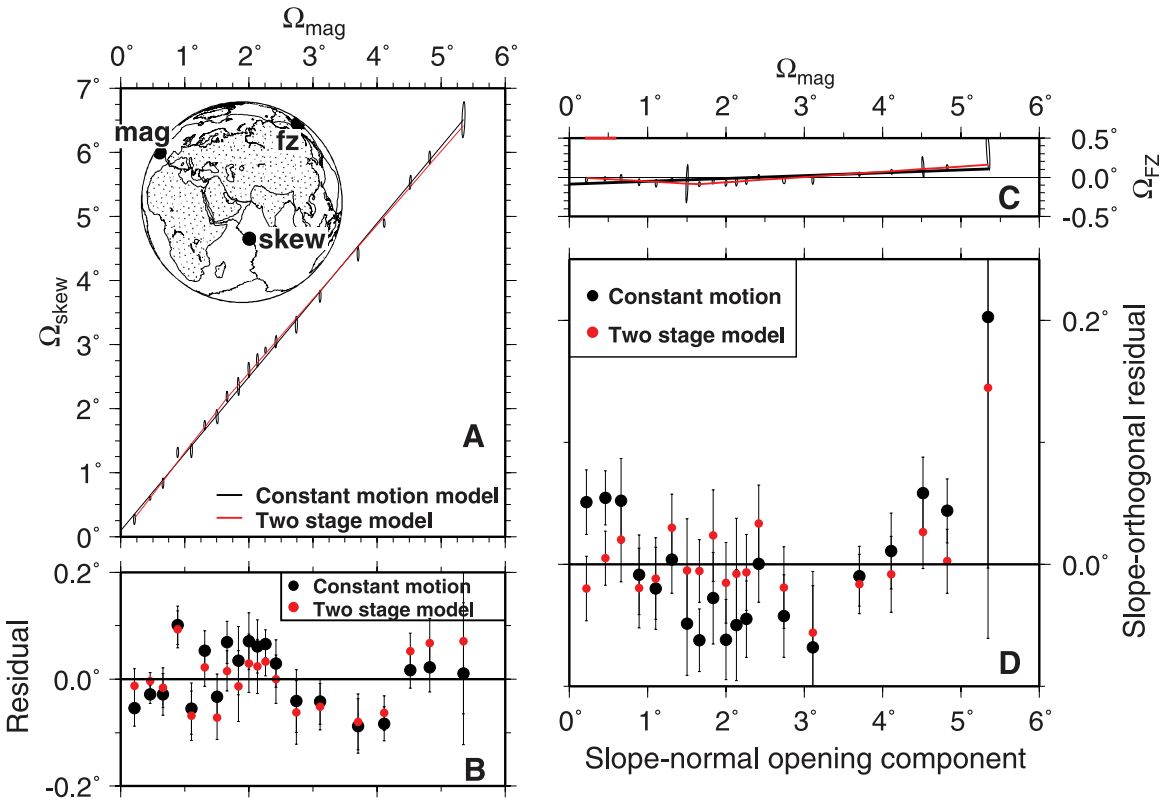

Figure 17. (a) Fit of single-line versus two-line least-distance fits for pure-opening versus skewed-fit orthogonal component pairs. (b) Residual angles for constant motion (black circles) and two-stage (red circles) models of pure-opening versus skewed-fit component pairs. (c) Constant motion (black line) versus two-stage (red line) fits for fracture zone versus pure-opening orthogonal angles. (d) Residual angles for constant motion (black circles) and two-stage (red circles) models of pure-opening versus fracture-zone component angles. For both sets of angle pairs, the two-stage model assumes that motion changed at 6.7 Ma, corresponding to the model that minimizes the combined misfit for the pure-opening versus skewed-fit and pure-opening versus fracture zone component pairs. The residual angles shown in Figures 17b and 17d are defined in a direction orthogonal to the best-fitting slopes.

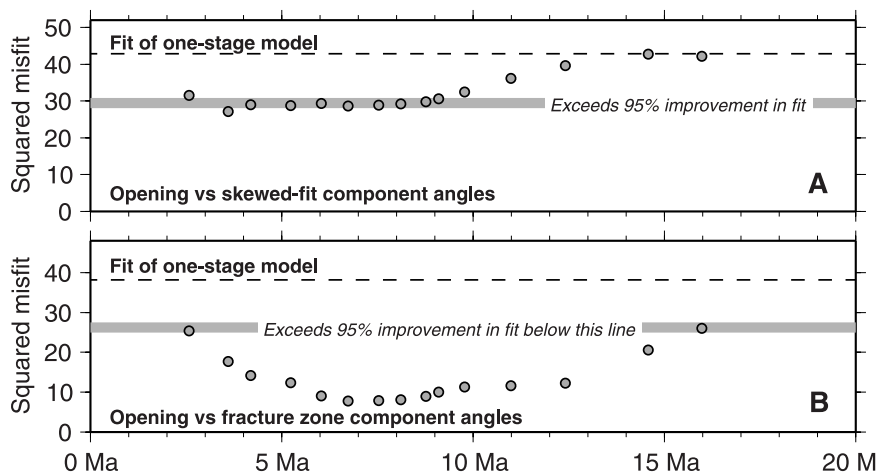

Figure 18. Comparison of least-squares misfits for one-stage and two-stage models of India-Somalia motion. Shaded circles show least-squares misfits for two-stage models, in which data younger than or equal to and older than the designated time are fit by separate slopes and intercepts. (a) Search for changes in ratio of opening to skew-fit component angles (see text). (b) Search for changes in ratio of opening to fracture zone component angles.

the spreading rate along the length of the India-Somalia boundary by 0.6 mm yr^{-1} per 1000 km of ridge length, (3) India-Somalia slip directions rotated 5–10° counterclockwise over the past 20 Myr, most likely at 11–9 Ma. Our data further suggest that the rotation pole and rate of angular opening have remained constant since 10–9 Ma within the tight bounds imposed by our data. In particular, our data suggest there has been a maximum variation of 2% in the rate of angular opening.

7.2. Comparison to Capricorn-Somalia Motion

[60] Using numerous data from the southern Central Indian ridge that record motion of the Capricorn plate relative to Somalia, DGR05 describe evidence for significant changes in Capricorn-Somalia motion at 8 ± 1 Ma, consisting of significant southeastward migration of the 20–8 Ma stage pole, clockwise rotation of the plate slip direction by 5–10°, and a transition to steady seafloor spreading. Our analysis of India-Somalia motion for the same period reveals remarkable similarities to Capricorn-Somalia motion and at least one important difference, as described below. To enable a more meaningful comparison of the relative motions of the Indian and Capricorn plates relative to Somalia, we first recalculated Capricorn-Somalia interval rates from DGR05 using the updated reversal ages from Table 1 (Figures 13 and 19).

[61] From 20–10 ± 1 Ma, Capricorn-Somalia and India-Somalia interval rates both decreased by ~12 mm yr^{-1}, equal to ~25–30% of their pre-slowdown opening rates. The spreading deceleration ended at 10 ± 1 Ma along both plate boundaries, since which spreading rates have been constant or nearly constant along both boundaries. Poles for both plate pairs shifted closer to their respective boundaries beginning no later than 11 Ma and ending by 9–8 Ma (Figure 19), albeit by significantly different amounts.

[62] There are several noteworthy differences in India-Somalia and Capricorn-Somalia kinematics since 20 Ma. The changes in pole locations along both plate boundaries at 11–9 Ma caused opposite-sense changes in plate slip directions, with India-Somalia directions rotating 5–10° counterclockwise and Capricorn-Somalia directions rotating 7° clockwise. These opposite-sense changes along the two plate boundaries corresponded with a significant acceleration of motion across the wide India-Capricorn plate boundary after ~8 Ma [*DeMets and Royer*, 2003; *DeMets et al.*, 2005]. The modest 3° southeastward shift from 11–9 Ma in the India-Somalia rotation pole with respect to the 20–9 Ma stage pole contrasts with a significantly larger ~15° southeastward shift of the Capricorn-Somalia pole with respect to its 20–8 Ma stage pole, which increased the spreading gradient by 3.9 mm yr^{-1} per thousand km of ridge length along the southern Central Indian ridge. Finally, a possible slow acceleration of Capricorn-Somalia spreading rates since 10 Ma (Figure 13b and Figure 19) has no counterpart along the India-Somalia boundary.

[63] The similarities described above suggests that the motions of the Indian and Capricorn plates are more tightly coupled than is implied by the DGR05 results. Significant differences however between the motions of these two plate pairs show that the torques acting on the Indian and/or Capricorn plates are not transmitted in their entirety across their wide plate boundary, thereby allowing the two plates to move independently. These observations substantiate the concept of composite plates [*Royer and Gordon*, 1997], which are composed of two or more physically contiguous but independently moving plates whose relative motions are strongly linked by mechanical coupling across their wide shared boundaries.

7.3. Implications for Forces Driving Indian Plate Motion

[64] One striking feature of the post-20 Ma evolution of India-Somalia and Capricorn-Somalia motions is their simultaneous slowdown in interval spreading rates between 20 Ma and 10 ± 1 Ma (Figure 19). We interpret the spreading rate slowdown as a passive response to the increasing work that was required to build topography at India's northern collisional boundary with Eurasia. Specifically, *Molnar and Lyon-Caen* [1988] postulate that progressively more work is required to raise mountain plateaus to ever higher elevations, reflecting the dependence of the amount of work that is needed to increase the gravitational potential of a plateau on the square of its height. Barring any change in the driving force(s) that pushed India northward between 20 Ma and 8 Ma, the time-progressive increase in work required to build the Tibetan plateau at India's northern boundary implies there was an increasing imbalance between the forces that drove and resisted Indian plate motion during this period. This in turn suggests that the northward component of the Indian plate's

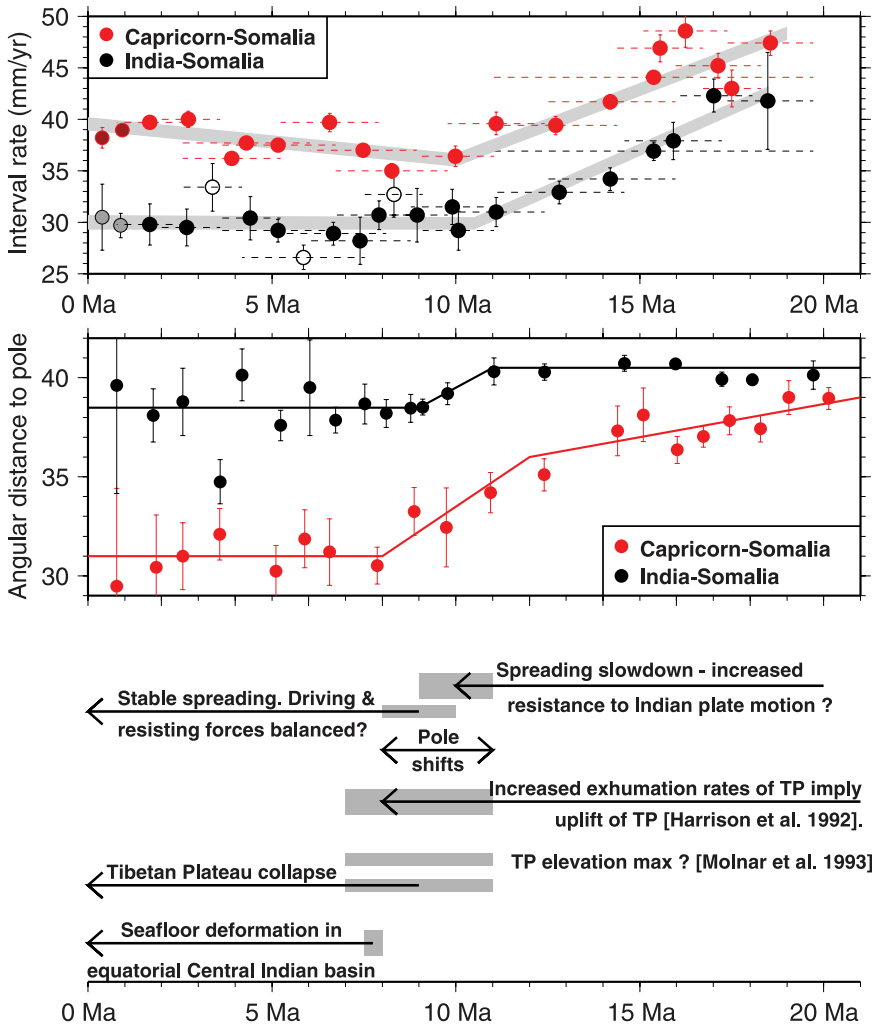

Figure 19. Comparison of (top) India-Somalia and Capricorn-Somalia interval opening rates and (bottom) rotation pole motion toward and away from their respective plate boundaries. Black and red lines summarize interpretations for the evolution of India-Somalia and Capricorn-Somalia motion described in text. Details regarding calculation of the interval rates are summarized in Figure 13.

absolute motion decreased from 20–8 Ma, resulting in slower seafloor spreading along the Indian plate's trailing edge.

[65] Between 11 Ma and 7 Ma, one and possibly two regional-scale tectonic events affected the Indian plate. Seafloor folding and faulting clearly initiated within a wide equatorial region south of India at ~7.5–8 Ma [*Eittreim and Ewing*, 1972; *Moore et al.*, 1974; *Weissel et al.*, 1980; *Curray and Munasinghe*, 1989; *Cochran*, 1990; *Krishna et al.*, 2001]. In addition, the Tibetan plateau may have attained its maximum elevation by ~8 Ma [*Harrison et al.*, 1992; *Molnar et al.*, 1993]. *Molnar et al.* [1993] demonstrate that if the Tibetan plateau reached elevations of 5.5–6 km before it collapsed, the deviatoric stresses directed outward from the plateau would likely have been high enough to induce folding of any thickly sedimented seafloor in the Central Indian basin. If uplift of the Tibetan plateau induced seafloor deformation south of India, the transition at 10–9 Ma from decelerating India-Somalia and Capricorn-Somalia seafloor spreading rates before that time to the present phase of steady spreading may indirectly record the time at which the Tibetan plateau attained its maximum elevation.

[66] The transition at 10–9 Ma to stable India-Somalia motion and nearly constant Capricorn-Somalia motion may be indirect evidence that the onset at 8 Ma of folding and faulting within the Central Indian basin fundamentally altered the preexisting balance between the forces that drove

and resisted Indian plate motion. A simple, but possibly applicable mechanical analogy for motion before 10–9 Ma may be a piston and cylinder, whereby subduction along the Java-Sumatra trench drove the Indian plate (the piston) to the north into the Himalayan convergence zone (the cylinder). Prior to 10–9 Ma, the difficulty of further increasing the height of the already-high Himalayan region may have been analogous to the increasing force required to drive a piston into an increasingly pressurized cylinder. Lacking an alternative mechanism for accommodating India's northward motion (e.g., a safety valve), this would have necessitated a slowdown in India's northward motion. The onset of folding and faulting across the diffuse oceanic plate boundary south of India at 8 Ma, possibly triggered by the attainment of a sufficiently large force-per-unit-length in the oceanic crust caused by the outward push of the high Tibetan plateau, added the equivalent of a pressure-triggered safety valve to the cylinder. Steady northward motion of the Indo-Australian composite plate thus resumed after 8 Ma and has since been accommodated by convergence across both the Indian plate's northern boundary and its diffuse boundaries with the Australian and Capricorn plates. Although the once rigid Indo-Australian plate has now broken into separate Indian, Capricorn, and Australian component plates, of which only the latter still subducts along the Java-Sumatra trench, strong coupling across their wide boundaries nonetheless maintains a steady northward push on the Indian plate that continues to drive orogeny in this region.

[67] If the small acceleration of Capricorn-Somalia spreading rates after ~9–10 Ma is real, it may be a passive response to the partial detachment at 8 Ma of the Indian and Capricorn plates across their wide equatorial boundary. This detachment presumably allowed the Capro-Australian composite plate to resume more rapid northeastward subduction along the Sumatra trench, leading to more rapid seafloor spreading along the spreading centers at the southern trailing edge of the Capricorn and Australian plates.

[68] If our speculations about the relationship between Indian plate kinematics and the evolving force balance between Indo-Australian plate subduction along Java-Sumatra trench and convergence at the edges of the Indian plate are correct, then our model makes several testable predictions. First, we predict that a similarly detailed analysis of seafloor spreading along the Southeast Indian ridge will uncover evidence for a slowdown in 20–8 Ma seafloor spreading rates, before motions of the Indian and Australian plates were decoupled by deformation across their diffuse equatorial boundary. We further predict the existence of a transition to steady or slightly accelerating spreading rates across the Southeast Indian ridge since 8 Ma, following the onset of deformation across the Indian plate's equatorial plate boundary.

8. Conclusions

[69] Dense Russian magnetic and bathymetric surveys of young seafloor along more than 90% of the India-Somalia plate boundary reveal important new characteristics about post-20 Ma India-Somalia motion, including the following: (1) Seafloor spreading rates between India and Somalia decreased by 30% from 20 Ma to 10 ± 1 Ma, possibly in response to increasing difficulty in accommodating crustal thickening within the Himalayan convergence zone. (2) The India-Somalia opening pole migrated toward the plate boundary from 11 Ma to 9 Ma, resulting in a modest increase in the along-axis gradient in seafloor spreading rates. (3) India-Somalia motion since ~10 has been remarkably steady, with variations in the rate of angular opening no greater than 2%. Similarities in India-Somalia and Capricorn-Somalia motion since 20 Ma indicate that their motions are more tightly coupled than previously recognized, substantiating the view that the Indian and Capricorn plates are part of a larger Indo-Australian composite plate. The coincidence in the timing of the several notable geotectonic events from 11–8 Ma, including the onset of faulting and folding of seafloor in the equatorial Central Indian basin, the possible attainment of maximum elevation of the Tibetan plateau, the apparent onset of plateau collapse, and a change to stable motion of the Indian and Capricorn plates relative to Somalia suggests they are related. Steady motion within the India-Somalia-Capricorn plate circuit since 8 Ma implies that the forces that drive and resist Indian plate motion have been in balance since 8 Ma. We suggest that convergence across the Himalayas and the wide India-Capricorn boundary south of India may act in tandem to maintain steady resistance to Indian plate motion in response to the subduction-driven, northward motion of the Indo-Australian composite plate.

[70] We also find evidence for at least two types of systematic error within the numerous anomaly crossings we use, one caused by correlated noise

specific to individual spreading segments and the second caused by systematic outward displacement of magnetic reversals along an entire plate boundary. Noise in the anomaly crossings is thus not purely Gaussian-distributed and random, contrary to an assumption often made in plate kinematic studies. Realistic rotation uncertainties that are generated via segment-based bootstrapping and post facto incorporation of additional systematic sources of bias into the rotation covariances exceed uncertainties that are propagated directly from the data errors by a factor of two or more.

Acknowledgments

[71] We thank Steve Cande, Peter Molnar, and Peter van Keken for constructive reviews of the manuscript. This work was supported by NSF International grant INT-0244894 (C.D.). Figures were drafted using GMT software [*Wessel and Smith*, 1991].

References

An, Z., J. E. Kutzbach, W. L. Prell, and S. C. Porter (2001), Evolution of Asian monsoons and phase uplift of the Himalaya-Tibetan plateau since late Miocene times, *Nature*, *411*, 62–66.

Atwater, T., and J. D. Mudie (1973), Detailed near-bottom geophysical study of the Gorda Rise, *J. Geophys. Res.*, *78*, 8665–8686.

Cande, S. C., and J. M. Stock (2004), Pacific-Antarctic-Australia motion and the formation of the Macquarie plate, *Geophys. J. Int.*, *157*, 399–414.

Chang, T. (1988), Estimating the relative rotation of two tectonic plates from boundary crossings, *JASA J. Am. Stat. Assoc.*, *83*, 1178–1183.

Cochran, J. R. (1990), Himalayan uplift, sea level, and the record of Bengal Fan sedimentation at the ODP leg 116 sites, *Proc. Ocean Drill. Program Sci. Results*, *116*, 397–414.

Curray, J. R., and T. Munasinghe (1989), Timing of intraplate deformation, northeastern Indian Ocean, *Earth Planet. Sci. Lett.*, *94*, 71–77.

DeMets, C., and J.-Y. Royer (2003), A new high-resolution model for India-Capricorn motion since 20 Ma: Implications for the chronology and magnitude of distributed crustal deformation in the Central Indian Basin, *Current Sci.*, *85*, 339–345.

DeMets, C., and D. S. Wilson (1997), Relative motions of the Pacific, Rivera, North American, and Cocos plates since 0.78 Ma, *J. Geophys. Res.*, *102*, 2789–2806.

DeMets, C., R. G. Gordon, and P. Vogt (1994), Location of the Africa-Australia-India triple junction and motion between the Australian and Indian plates: Results from an aeromagnetic investigation of the Central Indian and Carlsberg ridges, *Geophys. J. Int.*, *119*, 893–930.

DeMets, C., R. G. Gordon, and J.-Y. Royer (2005), Motion between the Indian, Capricorn, and Somalian plates since 20 Ma: Implications for the timing and magnitude of distributed deformation in the equatorial Indian Ocean, *Geophys. J. Int.*, *161*, 445–468.

Edmond, J. M., and Y. Huh (2003), Non-steady state carbonate recycling and implications for the evolution of atmospheric PCO_2, *Earth Planet. Sci. Lett.*, *216*, 125–139.

Efron, B., and R. Tibshirani (1986), Bootstrap method for standard errors, confidence intervals and other measures of statistical accuracy, *Stat. Sci.*, *1*, 54–77.

Eittreim, S., and J. Ewing (1972), Mid-plate tectonics in the Indian Ocean, *J. Geophys. Res.*, *77*, 6413–6421.

Fisher, N. I., T. Lewis, and B. J. J. Embleton (1993), *Statistical Analysis of Spherical Data*, 329 pp., Cambridge Univ. Press, New York.

Glebovsky, V. Y., et al. (1995), Mid-oceanic ridges and deep ocean basins: AMF structure, in *Anomalous Magnetic Field of the World Ocean*, edited by A. M. Gorodnitsky, pp. 67–144, CRC Press, Boca Raton, Fla.

Gordon, R. G., C. DeMets, and D. F. Argus (1990), Kinematic constraints on distributed lithospheric deformation in the equatorial Indian Ocean from present motion between the Australian and Indian plates, *Tectonics*, *9*, 409–422.

Gordon, R. G., C. DeMets, and J. Y. Royer (1998), Evidence for long-term diffuse deformation of the lithosphere of the equatorial Indian Ocean, *Nature*, *395*, 370–374.

Harrison, T. M., P. Copeland, W. S. F. Kidd, and A. Yin (1992), Raising Tibet, *Science*, *255*, 1663–1670.

Hellinger, S. J. (1979), The statistics of finite rotations in plate tectonics, Ph.D. thesis, 172 pp., Mass. Inst. of Technol., Cambridge.

Karasik, A. M., S. A. Mercuriev, L. I. Mitin, N. A. Sochevanova, and V. N. Yanovsky (1986), Peculiarities in the history of opening of the Arabian Sea from systematic magnetic survey data, *Dokl. Akad. Nauk SSSR*, *286*, 933–938.

Klootwijk, C. T., J. S. Gee, J. W. Peirce, and G. M. Smith (1991), Constraints on the India-Asia convergence: Paleomagnetic results from Ninetyeast ridge, *Proc. Ocean Drill. Program Sci. Results*, *121*, 777–881.

Krishna, K. S., J. M. Bull, and R. A. Scrutton (2001), Evidence for multiphase folding of the central Indian Ocean lithosphere, *Geology*, *29*, 715–718.

Lourens, L., F. J. Hilgen, J. Laskar, N. J. Shackleton, and D. Wilson (2004), The Neogene Period, in *A Geologic Time Scale 2004*, edited by F. Gradstein, J. Ogg, and A. Smith, pp. 909–440, Cambridge Univ. Press, New York.

Macdonald, K. C., S. P. Miller, B. P. Luyendyk, T. M. Atwater, and L. Shure (1983), Investigation of a Vine-Matthews magnetic lineation from a submersible: The source and character of marine magnetic anomalies, *J. Geophys. Res.*, *88*, 3403–3418.

Merkouriev, S. A., and N. A. Sotchevanova (2003), Structure and evolution of the Carlsberg Ridge: Evidence for non-stationary spreading on old and modern spreading centers, *Current Sci.*, *85*, 334–338.

Molnar, P. (2005), Mio-Plicene growth of the Tibetan plateau and evolution of East Asian climate, *Palaeontol. Electron.*, *8*, *2A*, 23 pp.

Molnar, P., and H. Lyon-Caen (1988), Some simple physical aspects of the support, structure, and evolution of mountain belts, *Spec. Pap. Geol. Soc. Am.*, *218*, 179–207.

Molnar, P., F. Pardo-Casas, and J. Stock (1988), The Cenozoic and Late Cretaceous evolution of the Indian Ocean basin: Uncertainties in the reconstructed positions of the Indian, African, and Antarctic plates, *Basin Res.*, *1*, 23–40.

Molnar, P., P. England, and J. Martinod (1993), Mantle dynamics, uplift of the Tibetan plateau, and the Indian monsoon, *Rev. Geophys.*, *31*, 357–396.

Moore, D. G., J. R. Curray, R. W. Raitt, and F. J. Emmel (1974), Stratigraphic-seismic section correlations and implications to Bengal Fan history, *Initial Rep. Deep Sea Drill. Proj.*, *22*, 403–412.

Patriat, P., and J. Achache (1984), India-Eurasia collision chronology has implications for crustal shortening and driving mechanism of plates, *Nature*, *311*, 615–621.

Patriat, P., and J. Segoufin (1988), Reconstruction of the central Indian Ocean, *Tectonophysics*, *155*, 211–234.

Raymo, M. E., and W. F. Ruddiman (1992), Tectonic forcing of late Cenozoic climate, *Nature*, *359*, 117–122.

Roest, W. R., J. Arkani-Hamed, and J. Verhoef (1992), The seafloor spreading rate dependence of the anomalous skewness of marine magnetic anomalies, *Geophys. J. Int.*, *109*, 653–669.

Royer, J.-Y., and T. Chang (1991), Evidence for relative motions between the Indian and Australian plates during the last 20 Myr from plate tectonic reconstructions: Implications for the deformation of the Indo-Australian plate, *J. Geophys. Res.*, *96*, 11,779–11,802.

Royer, J. Y., and R. G. Gordon (1997), The motion and boundary between the Capricorn and Australian plates, *Science*, *277*, 1268–1274.

Royer, J.-Y., R. G. Gordon, C. DeMets, and P. R. Vogt (1997), New limits on the motion between India and Australia since chron 5 (11 Ma) and implications for lithospheric deformation in the equatorial Indian Ocean, *Geophys. J. Int.*, *129*, 41–74.

Sandwell, D. T., and W. H. F. Smith (1997), Marine gravity anomaly from Geosat and ERS 1 satellite altimetry, *J. Geophys. Res.*, *102*, 10,039–10,054.

Schouten, H., and K. McCamy (1972), Filtering marine magnetic anomalies, *J. Geophys. Res.*, *77*, 7089–7099.

Sempere, J.-C., K. C. Macdonald, and S. P. Miller (1987), Detailed study of the Brunhes/Matuyama reversal boundary on the East Pacific Rise at 19°30′S: Implications for crustal emplacement processes at an ultra fast spreading center, *Mar. Geophys. Res.*, *9*, 1–23.

Stock, J. M., and P. Molnar (1983), Some geometrical aspects of uncertainties in combined plate reconstructions, *Geology*, *11*, 697–701.

Weissel, J. K., R. N. Anderson, and C. A. Geller (1980), Deformation of the Indo-Australian plate, *Nature*, *287*, 284–291.

Wessel, P., and W. H. F. Smith (1991), Free software helps map and display data, *Eos Trans. AGU*, *72*, 441–446.

Wiens, D. A., et al. (1985), A diffuse plate boundary model for Indian Ocean tectonics, *Geophys. Res. Lett.*, *12*, 429–432.

Wilson, D. S. (1993), Confidence intervals for motion and deformation of the Juan de Fuca plate, *J. Geophys. Res.*, *98*, 16,053–16,071.